SYNTHESIS OF GRAPHITIC CARBON NITRIDE (g-C$_3$N$_4$) / COCONUT SHELL HUSK DERIVED-CARBON COMPOSITE FOR SONOCATALYTIC DEGRADATION OF ORGANIC DYE

AARON KOE ZHEN YAO

A project report submitted in partial fulfilment of the requirements for the award of Bachelor of Engineering (Honours) Chemical Engineering

Lee Kong Chian Faculty of Engineering and Science
Universiti Tunku Abdul Rahman

April 2019

DECLARATION

I hereby declare that this project report is based on my original work except for citations and quotations which have been duly acknowledged. I also declare that it has not been previously and concurrently submitted for any other degree or award at UTAR or other institutions.

Signature   :   _____

Name   :   AARON KOE ZHEN YAO

ID No.   :   14UEB01446

Date   :   _____

APPROVAL FOR SUBMISSION

I certify that this project report entitled **"SYNTHESIS OF GRAPHITIC CARBON NITRIDE (g-C$_3$N$_4$) / COCONUT SHELL HUSK DERIVED-CARBON COMPOSITE FOR SONOCATALYTIC DEGRADATION OF ORGANIC DYE"** was prepared by **AARON KOE ZHEN YAO** has met the required standard for submission in partial fulfilment of the requirements for the award of Bachelor of Engineering (Honours) Chemical Engineering at Universiti Tunku Abdul Rahman.

Approved by,

Signature   :   _____

Supervisor   :   DR. PANG YEAN LING
                    _____

Date   :   _____

Signature   :   _____

Co-Supervisor   :   DR. STEVEN LIM
                    _____

Date   :   _____

ACKNOWLEDGEMENTS

ABSTRACT

Pure graphitic carbon nitride (g-C$_3$N$_4$), pure carbon, and carbon/g-C$_3$N$_4$ composite at different weight percentages were prepared and characterised by using X-ray diffraction (XRD), scanning electron microscopy-energy dispersive X-ray (SEM-EDX), and fourier-transform infrared (FTIR) analysis. The addition of carbon to carbon/g-C$_3$N$_4$ composites resulted in a loss of the XRD characteristic peaks of pure g-C$_3$N$_4$. The SEM images illustrated pure g-C$_3$N$_4$ possessed irregular shape and irregular porous structure. For the composite samples, the irregular-shaped particles were decreased as increasing the carbon weightage. The EDX results showed that the pure g-C$_3$N$_4$ had a carbon to nitrogen ratio of 0.78 which was close to the stoichiometric ratio of 0.75. The FTIR results obtained was complementary to the XRD patterns observed. The effect of carbon amount (1 wt%, 5wt%, 10 wt%, 15 wt%, 20 wt%, and 25 wt%) in carbon/g-C$_3$N$_4$ composites was studied and 10 wt% C/g-C$_3$N$_4$ showed the best catalytic activity. The organic dye (Malachite Green) with the best degradation performance among Malachite Green, Methyl Orange, and Acid Orange G was chosen for the parameter studies due to its characteristic of cationic dye while the surface charge of the catalyst was negative at the natural solution pH. The effect of hydrogen peroxide (H$_2$O$_2$) dosage on the sonocatalytic degradation efficiency of Malachite Green was also studied. Although the incorporation of H$_2$O$_2$ increased the degradation efficiency of Malachite Green, it was decided that no H$_2$O$_2$ should be used to avoid the usage of toxic chemical. The optimisation study was conducted by using Design Expert 11 with a Central Composite Design (CCD) model. Three factors which were initial dye concentration (20 to 25 ppm), initial catalyst loading (0.3 to 0.5 g/L), and solution pH (4 to 8) were studied for this model. The model was validated by using the optimum conditions (initial dye concentration = 20 ppm, initial catalyst loading = 0.5 g/L, solution pH = 8 for 10 minutes) obtained from the model. By comparing the actual degradation efficiency of Malachite Green (97.11 %) with the predicted value (96.69 %) from the model, it was found that the percentage error between both values were only 0.43 %. The reusability study of 10 wt% C/g-C$_3$N$_4$ was also studied. The reused sample showed high degradation performance even after three catalytic cycles. In short, 10 wt% C/g-C$_3$N$_4$ has high potential for industrial application since it is cost effective, reusable, sustainable, and provides good degradation performance.

TABLE OF CONTENTS

LIST OF TABLES

LIST OF FIGURES

LIST OF SYMBOLS / ABBREVIATIONS

$C = O$	carbonyl group
$C/g\text{-}C_3N_4$	carbon/graphitic carbon nitride composites
C_0	initial dye concentration, mg/L
C-dots	carbon dots
CdS	cadmium sulphide
CNDs	carbon nanodots
CN-T	thiourea graphitic carbon nitride
CN-U	urea graphitic carbon nitride
CO_2	carbon dioxide
CQDs	carbon quantum dots
C_t	dye concentration at time t, mg/L
e^-	electrons
$g\text{-}C_3N_4$	graphitic carbon nitride
$H\bullet$	hydrogen radical
H	hydrogen atom
h^+	holes
H^+	hydrogen ions
H_2O	water
H_2O_2	hydrogen peroxide
HCl	hydrochloric acid
n	number of variables
-N=N-	azo dyes
NaOH	sodium hydroxide
$O_2^-\bullet$	superoxide ion
O_2	oxygen
OH	hydroxyl
$\bullet OH$	hydroxyl radical
$OOH\bullet$	hydroperoxyl radical
R^2	coefficient of determination
TiO_2	titanium dioxide
X_1	initial dye concentration
X_2	initial catalyst dosage

X_3	solution pH
ZnO	zinc oxide
α	distance of each axial point from the centre in CCD
ANOVA	analysis of variance
AOPs	advanced oxidation processes
BET	Brunauer-Emmett-Teller
BOD	biochemical oxygen demand
CB	conduction band
CB	conduction band
CCD	central composite design
COD	chemical oxygen demand
DO	dissolved oxygen
DoE	design of expert
DS	dissolved solid
FTIR	fourier-transform infrared
HOMO	highest occupied molecular orbitals
LUMO	lowest unoccupied molecular orbitals
NH_3-N	ammoniacal nitrogen
RSM	response surface methodology
SEM-EDX	scanning electron microscopy-energy dispersive X-ray
SL	sonoluminescence
SS	suspended solid
UV	ultra-violet
UV-Vis	ultraviolet-visible-infrared
VB	valence band
XRD	X-ray diffraction

LIST OF APPENDICES

CHAPTER 1

INTRODUCTION

1.1   Water Pollution and Scarcity in Malaysia

Malaysia is a developing country that is currently experiencing economic growth with a rapid transition to an urban and industrialised society. This change has created many environmental problems and one of it is the increase in discharge of wastewater that would lead to serious water pollution problem in Malaysia (Goh and Ismail, 2018). Water pollution affects the welfare of all living things, including humans, the economy of the country and it contributes greatly on sustainability of water resource (Afroz and Rahman, 2017). This implies that the discharge of untreated wastewater will cause major environmental issues and must be monitored strictly. Two different sources for water pollution, which are namely point source and non-point source (Afroz and Rahman, 2017). Point source are pollution sources that are easily traceable. The wastewater generated come from network of pipes that are originated from industrial discharges and sewage treatment plants. Non-point sources are water pollution that are not easily traced back to the root cause. Urban and agricultural runoff are examples of non-point sources. Quality of water is determined by a few parameters which are dissolved oxygen (DO), chemical oxygen demand (COD), biochemical oxygen demand (BOD), ammoniacal nitrogen (NH_3-N), and suspended solids (SS) present in the water (Afroz and Rahman, 2017).

Figure 1.1 shows the number of rivers polluted by three separate pollutants, which are BOD, SS and NH_3-N. The collected data are based on the 140 rivers monitored by the department. The data shows that the number of rivers polluted by BOD is extremely high. The number of rivers polluted by BOD increases rapidly from the year 2013 to 2014. Although there is a slight drop in 2015, the number of rivers polluted by BOD rose back up to 129 in 2016 (DOE, 2016). This is not a good sign as high BOD will affect water quality and reduce the availability of freshwater supply. The remaining pollutants does not pollute as much rivers as BOD. This implies that the water pollution caused by BOD in Malaysia is at a chronic state and actions must be taken immediately to overcome this environmental issue.
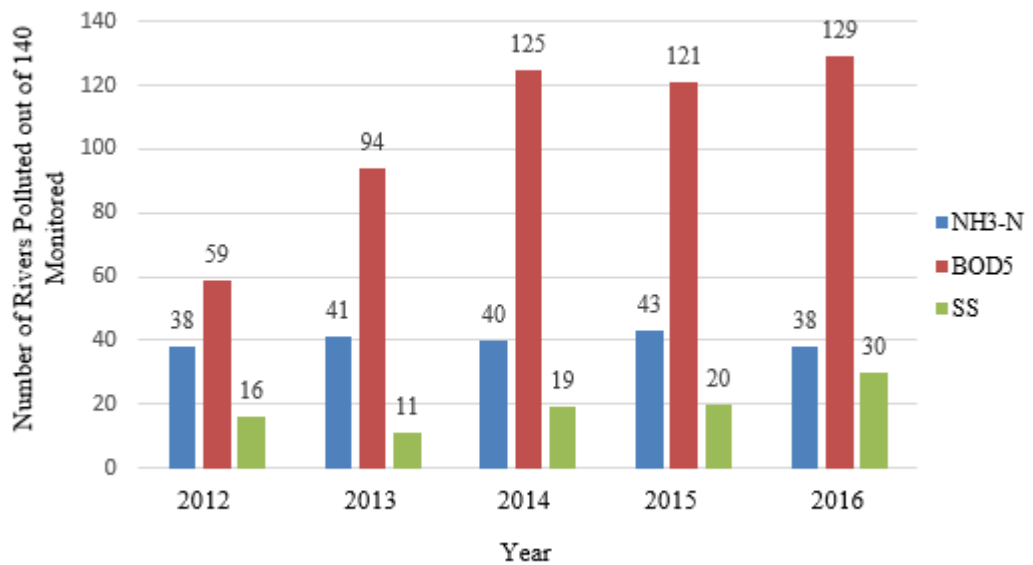
Figure 1.1: Graph of Number of Rivers Polluted by Specific Pollutants Out of 140 Rivers Monitored Against Year (DOE, 2016).

The demand for water is higher at a more populated area (Oh, et al., 2018). Figure 1.2 shows the number of establishments that deals with water supply, sewerage, wastewater management and remediation activities by different states in 2015. The number of establishments in city-like states are much greater than the other rural states. The total number of establishments in Malaysia recorded is 784 (DOS, 2011). For example, Pulau Pinang has 68 establishments while Kelantan has only 4 establishments despite the huge difference in land resources (DOS, 2011). The large contrast in number of establishments is due to the dense population and urbanization of Pulau Pinang. Most of these establishments are located in Selangor. Piarapakaran 2018 reported on News Straight Times that Selangor is having major problems in water scarcity. This is due to the low treated water reserve margin. This implies that even though the number of establishments are the largest in Selangor, water scarcity is still a major problem due to the higher demand caused by urbanization.
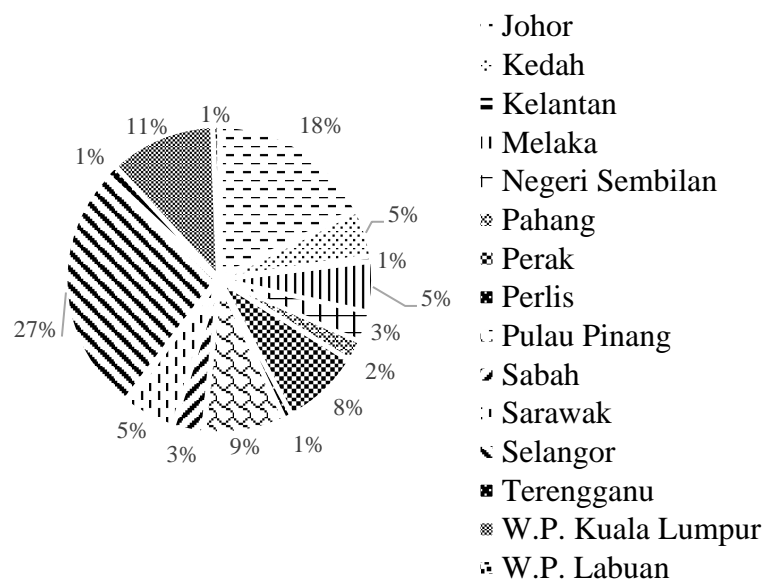
Figure 1.2: Number of Establishments that Deals with Water Supply, Sewerage, Wastewater Management and Remediation Activities by Different States in 2015 (DOS, 2011).

Water shortage might impose a major problem not only in Selangor but to the whole country in the future. An estimation from United Nations states that many countries around the globe will face water stress or draught in the coming decade (Goh and Ismail, 2018). Malaysia would be one of the countries stated if counter measures are not pursued rapidly. The treatment of wastewater is an important matter for environmental and social sustainability. Wastewater treatment have two main functions. The main function of wastewater treatment is to ensure that the discharge will not have such a great impact on the water quality and aquatic life. The second function of wastewater treatment is to reuse the wastewater that is treated. This function is focused on combating water scarcity in the world. The current industries are being pushed to focus on cleaner production technology such as recovery and recycling of water (Mokhtar, et al., 2015). With the implementations of the 17 Sustainable Development Goals, clean water and sanitation has increased in importance to raise the quality of living and reduce the environmental impact. The treated wastewater in Malaysia must achieve the minimum standard that is implemented by the Department of Environment as shown in Table 1.1.

Table 1.1: The Acceptable Conditions of Sewage Discharge of Standards A and B (DOE, 2010)

Parameter	Unit	Standard*	
		A	B
Temperature	^{O}C	40	40
Solution pH	-	6.0-9.0	5.5-9.0
BOD$_5$ at 20 ^{O}C	mg/L	20	50
COD	mg/L	120	200
Suspended Solids	mg/L	50	100
Ammonical Nitrogen	mg/L	5.0-10.0	5.0-20.0

*Standard A refers to the for discharges into any inland waters within listed catchment areas. Standard B refers to the other inland or Malaysian waters.

1.2 Characteristics of Textile Industry Effluent

Textile materials are very popular due to their low production cost and great mechanical properties (Liu, et al., 2018). In textile industry, dye is extensively used in every stage of the production process to colorize the products (Ashfaq and Khatoon, 2014). The downside for textile materials is the huge environmental impact caused by the discharge of effluent from the production process. The effluents contain non-biodegradable dyes and other chemicals which are toxic and poses a serious threat to fresh water. (Kaur, Kushwaha and Sangal, 2018) Table 1.2 summarises the types and characteristics of effluents from each stage in the manufacturing process of textiles.

Wastewater generated from textile industries are harmful to the environment because it contains contaminants such as organic matter, sulphide, oil, detergents, grease, soap and sodas (Cetinkaya, et al., 2018). The characteristics of wastewater being discharged from textile industries are shown in Table 1.3. The large range of values for colour parameter indicates that the pollution level in the textile wastewater.

These pollutants need to be eliminated from the wastewater by going through wastewater treatment method that utilises chemical, physical or biological treatment methods (Cetinkaya, et al., 2018). However, organic dyes are harder to treat due to their chemical stability and biological resistance (Kaur, Kushwaha and Sangal, 2018).

Table 1.2: Constituent and Characteristic of Discharge from Each Stage (Hossain, Sarker and Khan, 2018)

Stage	Constituent	Discharge Characteristic
Sizing	Wax, starch, waxing agent, caboxymethyl cellulose	High BOD, COD
Desizing	Fat, wax, starch, enzyme	High BOD, COD, SS, and dissolved solid (DS)
Bleaching	Sodium hypochlorite, hydrogen peroxide, chlorine, sodium phosphate, sodium silicate, acid, surfactant	High solution pH, SS
Mercerizing	Sodium hydroxide, cotton wax	Low BOD, high solution pH, DS
Dyeing	Colour, reducing agent, oxidizing agent, acetic acid	High BOD, DS, and heavy metal
Printing	Urea, oil, binder, reducing agent	High BOD, SS, and slightly alkaline
Finishing	Resin, catalyst, softener, fluorocarbon, inorganic salt	Low BOD, and slightly alkaline

Table 1.3: Textile Wastewater Characteristics (Ashfaq and Khatoon, 2014)

Parameters	Range of Values
Solution pH	7.0 - 9.0
Biochemical Oxygen Demand, mg/L	80 – 6000
Chemical Oxygen Demand, mg/L	150 – 12000
Total Suspended Solids, mg/L	15 – 8000
Total Dissolved Solids, mg/L	2900 – 3100
Chloride, mg/L	1000 – 1600
Colour, Pt-Co	50 – 2500

1.3   Problem Statement

Water pollution and scarcity is going to be a major problem in Malaysia for upcoming years. With the increasing number of polluted rivers in Malaysia, fresh water supply for domestic purposes will be limited (DOE, 2016). With the increase in population, water demand will rise along with the discharge of municipal wastewater. Organic or synthetic dyes displays significantly noticeable colour in the effluent even at low concentration. By blocking the light, aquatic plants cannot undergo photosynthesis which causes the DO level in the river to decrease and harm the ecosystem. Dyes are carcinogenic and toxic which will impose health and environmental problems (Gonawala and Mehta, 2014). Human that consume the water from these rivers will have increased risk of cancer and the toxic property of dyes will poison humans and even aquatic species.

With the world switching towards a more sustainable technology, sonocatalytic technology of wastewater treatment is in the limelight due to their environmental-friendly and green wastewater treatment method (Yu, et al., 2018). The common semiconductor used for these treatment methods are titanium dioxide (TiO_2). TiO_2 has disadvantages of a wide band gap energy that results in unsatisfactory performance (Yu, et al., 2018). Since the main focus of treating the wastewater is to overcome water scarcity and pollution, a metal-free semiconductor is chosen for this research. Graphitic carbon nitride ($g-C_3N_4$) is a of metal-free sonocatalyst that was discovered recently. With it being metal-free, the cost of this semiconductor will be cheaper than TiO_2 due to the abundance and renewability of raw materials. The main drawback of $g-C_3N_4$ is the high recombination rate of photo-induced carriers, which can be improved by incorporating carbon materials (Yu, et al., 2018). Thus, this research focus on the carbon material that are obtained from coconut shell husks. The utilisation of unwanted husks as carbon material can reduce and reuse this type of biomass. $G-C_3N_4$ doped with carbon derived from coconut shell husk will be a green material since the raw materials used are not hazardous.

1.4   Aims and Objectives

The main objective of this study was to investigate the sonocatalytic degradation efficiency of organic dyes in the presence of $g-C_3N_4$ composited with carbon. In order to achieve this objective, the following sub-objectives were identified:

1. To synthesise and characterise g-C$_3$N$_4$/ coconut shell husk derived carbon.

2. To determine the optimum condition for sonocatalytic degradation of organic dyes in the presence of g-C$_3$N$_4$/ coconut shell husk derived carbon under different operating parameters.

1.5   Scope and Limitation of the Study

The scope of this study was designed to achieve the objectives. Pure carbon is prepared by pyrolysis of coconut shell husk at a temperature of 750 ^{O}C for 1 hour and then grinded to carbon powder that has a size of 100 μm. Pure g-C$_3$N$_4$ and carbon/g-C$_3$N$_4$ composite at different weight percentage are prepared by heating pure urea and the carbon and urea mixture at 500 ^{O}C for 2 hours. The samples prepared are characterised by using X-ray diffraction (XRD), scanning electron microscopy-energy dispersive X-ray (SEM-EDX) and fourier-transform infrared (FTIR).

The optimum condition for various parameters will also be investigated. The various parameters include the amount of carbon composited with g-C$_3$N$_4$, type of organic dye, and H$_2$O$_2$ dosage. The optimisation study will be conducted by using Design Expert 11 with a Central Composite Design (CCD) model. The model will take into account three factors which are the initial dye concentration, initial catalyst loading, and solution pH. The reusability study for the sample with the best degradation performance will also be studied.

The limitation of this study is the lack of surface area for the samples prepared. The surface area of the samples should be characterised by using Brunauer-Emmett-Teller (BET) surface analysis. With the specific surface area for every sample, the variation in degradation performance can be explained in detail.

1.6   Contribution of the Study

This study focuses on the preparation and sonocatalytic degradation performance of pure g-C$_3$N$_4$, pure carbon, and carbon/g-C$_3$N$_4$ composite at different weight percentage. This study will show whether the preparation method for the samples is effective or not by studying the characteristic and degradation performance of the samples. The implementation of eco-friendly raw materials introduces a more sustainable catalyst for the wastewater treatment process. The raw materials used in this study are also cost-effective which makes the utilisation of the studied samples to have more practicality.

The study on various parameters will help determine the optimum carbon amount that should be composited with g-C_3N_4 to obtain the best degradation efficiency. Not only that, the optimum conditions such as type of organic dye, H_2O_2 dosage, initial dye concentration, initial catalyst loading, and solution pH will also be determined in this study for the best degradation performance for practical use. The reusability of the sample with the best degradation performance will also be conducted. If the sample is found to be reusable, it will be more cost-effective which is favourable for industrial application.

1.7   Outline of the Report

This report consists of five chapters which are the introduction, literature review, methodology and work plan, results and discussion, and conclusion and recommendation.

Chapter 1 is a brief introduction on the water pollution and scarcity in Malaysia. This chapter shows the statistics that are found from the Department of Environment. The characteristic of textile industry effluent is also briefly studied.

Chapter 2 contains the literature review done for this report. Since the target pollutant for this report is organic dye, the classification of dyes and the basis for colour of dyes are discussed. The available textile wastewater treatment methods are also studied. This report focuses on the sonocatalytic degradation of pure g-C_3N_4, pure carbon, and carbon/g-C_3N_4 composite at different weight percentage. The theory behind sonocatalysis and the properties of the pure and incorporated samples are also discussed in chapter 2. The theoretical effect of various parameters on the degradation efficiency was also researched along with the implementation of Design Expert 11.

Chapter 3 shows the methodology and work plan for the lab work. This chapter consists of the materials, chemicals, and equipment used for the experiment conducted. A flowchart and experimental set up was also included in this chapter. The value of the constant variables when experimenting on the various parameters are also indicated in chapter 3. The experimental matrix for the optimisation study from Design Expert 11 is also shown in chapter 3. The procedure for reusability study and the calculation for liquid-sample analysis can also be found in chapter 3.

Chapter 4 includes the results and discussion obtained from the experimental work that will be done. The characterisation of samples by XRD, SEM-EDX, and FTIR will be included in this chapter. The optimum condition of various parameters

and the optimisation study that will be conducted will also be discussed here. The reusability study for the optimum sample and the possible mechanism of the degradation will be shown at the end of the chapter.

The last chapter which is chapter 5 shows the conclusion and recommendations of the report.

CHAPTER 2

LITERATURE REVIEW

2.1   Classification of Dyes
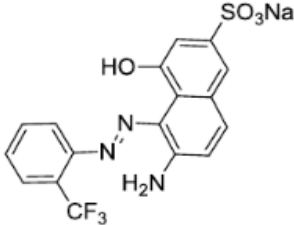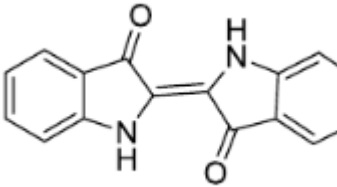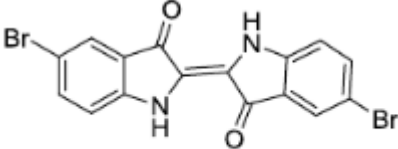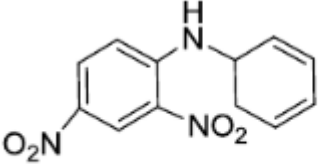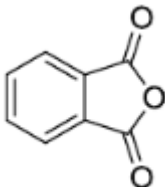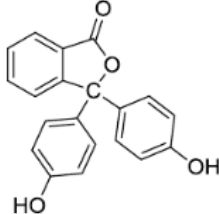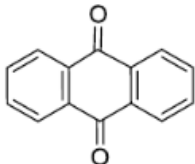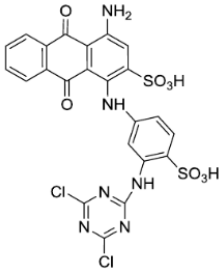
Dyes are substances with colour where the type of colour is based on the chemical structure that the dye possess (Gürses, et al., 2016). Dyes can be classified based on their source, chemical structure, and application methods.

There are two main sources for dyes which are natural and synthetic. Natural dyes are derived from animals, plants, and minerals (Gürses, et al., 2016). The raw materials to produce natural dyes are obtained from natural sources. For natural dyes to be applied on textiles, mordants will be required. The fixation of natural dyes on textile can be achieved by mordant because it is a metallic salt that have attraction for the fibres and natural dyes (Benkhaya, Harfi and Harfi, 2017). Transition metal ions show strong affinity for the textile and the natural dye which makes them good mordants for natural dyes fixation (Kumar and Konar, 2011). The source for synthetic dyes are obtained from petroleum compounds (Gürses, et al., 2016). Synthetic dyes sare available at very affordable prices and in various colours and colour shades. This causes synthetic dye to be more favourable in industries as compared to the eco-friendlier natural dye. Although the production of synthetic dyes is not that costly, synthetic dye may cause skin allergies and the production process produces hazardous by-products. This means that synthetic dyes will harm the welfare of humans and the environment.

The classification of chemical structures is based on the chromophores present in the structure of the dye. The structural part of molecules that allows dyes to have colour is the presence of chromophores because chromophores can absorb the visible light spectrum. The classification of dyes based on their chromophores are displayed in Table 2.1. Azo dyes that consists of N to N double bonds are the largest class of synthetic dyes.

The last type of classification will be based on the application methods of the dyes. For this classification, dyes can be classified into various classes namely, reactive dyes, disperse dyes, direct dyes, vat dyes, basic dyes, acid dyes, and solvent dyes. These classes can be further categorised into water-soluble and water-insoluble dyes.

Table 2.1: Classification of Dyes Based on Chromophores (Benkhaya, Harfi and Harfi, 2017)

Dye Class	Chromophore	Example
Azo Dyes		Acid Red 337
Indigoid Dyes		C.I. Vat Blue 35
Nitro Dyes		Disperse yellow 14
Phthalein Dyes		Phenolphtaleine
Anthraquinone Dyes		Reactive Blue 4

The dyes that are water-soluble are direct dyes, basic dyes, and acid dyes. Water-insoluble dyes are made up of the rest of the listed dyes which are disperse dyes, vat dyes, and solvent dyes. Water-soluble dyes will be applied to materials that are hydrophilic while water-insoluble dyes will be used on hydrophobic materials. Table 2.2 states the method of application from different classes of dye.

Table 2.2: Method of Applications Based on Dyes Class (Hunger, 2002)

Class	Principal Substrates	Method of Application
Reactive	Silk, wool, cotton and nylon	Reactive site on dye reacts with functional group on fibre for dye to be bounded under pH and heat influence.
Disperse	Polyamide, acetate, acrylic, polyester and plastic	Fine aqueous dispersions that can be padded on cloth and baked.
Direct	Paper, cotton, rayon, leather and nylon	Applied from slightly alkaline or neutral baths which containing additional electrolyte.
Vat	Rayon, cotton and wool	Water-insoluble dyes solubilized by reducing with sodium hydrogensulfide, then exhausted on fiber and reoxidized.
Basic	Modified nylon, polyester, inks, paper and polyacrylonitrile	Applied in acidic dyebaths
Acid	Wool, silk, paper, inks, leather and nylon	Usually applied from neutral to acidic dyebaths
Solvent	Gasoline, plastics, varnishes, stains, inks, fats, oils, lacquers and waxes	Dissolution in the substrate

2.2 Basis for Colour of Dyes

Dyes can have unique colours based on a few factors. The first factor is that dye possesses chemical structure that can absorb light with wavelength in the range of 400 to 700 nm. Different wavelengths absorbed will display different colours. The list of colours that are observed and absorbed are listed in Table 2.3. The range of wavelength is the visible spectra. Secondly, the component must have one or more than one chromophore to be classified as dye. Possessing a conjugated system is the third factor that causes dye to show colour (Lyon, 2010). A conjugated system would mean that it must have double and single bonds that can be alternated. The last factor that is required is that the dye exhibits resonance of electrons. These four factors are crucial for a dye to be displayed colours, without any one of them will render the dye colourless.

Table 2.3: The Wavelength Absorbed with the Colour Observed on Dyes (Lyon, 2010)

Wavelength Absorbed, nm	Colour Observed on Dye
400 – 435	Greenish yellow
435 – 480	Yellow
480 – 490	Orange
490 – 500	Red
500 – 560	Purple
560 – 580	Violet
580 – 595	Blue
595 – 605	Blueish green
605 – 700	Greenish blue

Other than chromophores, colour helpers will also be found in dyes. These colour helpers are known as auxochromes. The auxochromes exists in the form of hydroxyl, amino, carboxylic acid, and sulfonic acid groups. The presence of these groups are not the crucial factors for colour possession in dyes. Auxochromes can shift the colour that is being observed and also effect the dye solubility since these groups are mostly hydrophilic (Lyon, 2010).

2.3   Textile Wastewater Treatment Methods

Currently, various methods are being implemented to treat coloured wastewater. The methods can be categorised into three main methods namely physical, biological and chemical treatment methods.

2.3.1   Physical Treatment

Physical treatment method normally uses adsorption or membrane filtration to remove colour from the textile wastewaters. Coagulation and flocculation techniques are also a part of the physical treatment for dyes.

Adsorption treatment method removes dyes through the contact between the target pollutants and the surface of the adsorbent (Joshi, Bansal and Purwar, 2003) This method is the most commonly used method for tertiary treatment in textile industries. The adsorbents are mostly porous solid, which indicated that they possess high surface area to enable the organic dyes to be removed by adsorbing on the surface of the adsorbents. When the adsorbed adsorbent reach full saturated state, it can then be replaced or regenerated. Surface area, size of dye, solution, temperature, pH of solution, contact time and the interaction between dye and surface are crucial factors that can affect the performance of an adsorbent (Saini, 2017). Activated carbon is a very popular adsorbent due to its high surface area. Bio-sorbents are potential alternatives due to their low cost and renewability. The main drawback of adsorption method is related to the short lifespan of the adsorbent. It has to be regenerated or replaced from time to time depending on how polluted of the wastewater is.

Membrane separation can purify and improve the quality of the final product. It uses a semi-permeable wall to separate the targeted pollutants with the wastewater. Membrane separation has four different categories, which are nano-filtration, ultra-filtration, reverse osmosis, and micro-filtration. Membrane separation has a high efficiency of separation which will provide clean liquid effluent and raw material recovery (Joshi, Bansal and Purwar, 2003). The removed dye can be removed from the membrane and reused again to save cost. The main disadvantage for this method is the membrane fouling that will greatly decrease the efficiency of the membrane.

The coagulation and flocculation method provide the most economical method to remove organic pollutants compared to adsorption and membrane separation. This method is usually paired with a sedimentation tank where the flocs will be given time to settle to the bottom of the tank and be removed from the water through gravity.

Coagulants are added to allow the impurities in the water to be attracted to each other to form a larger clump of molecules. This will increase the weight of the molecules and will cause them to be removed by gravity. This treatment might increase the total dissolved solids level of the wastewater which hinders the reusability of the treated water (Joshi, Bansal and Purwar, 2003). This is not favorable since the treated water is expected to be clean and available for use to create a sustainable environment.

The physical treatment methods remove dyes by literally separating them from the wastewater. The pollutants that are removed will still be in the form which they are discharged. The main drawback of physical treatment method is the formation of sludge from the removal of pollutants. This sludge must still be treated again before disposal since it will be very concentrated with the pollutant.

2.3.2   Biological Treatment

There are only two categories for biological treatment which is aerobic biological treatment and anaerobic biological treatment.

Aerobic treatment requires the presence of oxygen (O_2). This treatment is not that effective since dyes are made to resist oxidative biodegradation. This will cause the degradation of textile wastewater to progress at a much slower rate compared to normal domestic wastewater (Joshi, Bansal and Purwar, 2003). The aerobic microorganisms will be introduced to the wastewater in the form of an activated sludge. Several researches have shown that the major contributor to this type of the removal of dyes is due to the activated sludge. Dyes will be adsorbed on the activated sludge rather than be biodegraded by the aerobic microorganism. Therefore, aerobic treatment of dyes is not an effective treatment.

Anaerobic treatment operates in the absence on O_2 by using anaerobic microorganisms. Anaerobic biological treatment will break down the organic dyes into amines while decolourising them. The amines produced are found to be very hazardous, making this treatment method undesired. Anaerobic treatment can be followed by aerobic biological treatment to degrade the amines that are produced by the anaerobic bacteria when dye is digested (Joshi, Bansal and Purwar, 2003). This anaerobic-aerobic treatment method will improve the colour reduction of the biological treatment methods greatly. Since anaerobic treatment alone is insufficient to treat organic dyes effectively, the combination of biological treatment with other methods are applied.

Biological treatment methods have very low operating costs. The anaerobic method can produce biogas from digestion which can be used as fuel, which will greatly decrease cost (Saini, 2017). Biological treatment methods require a large area to treat the wastewater. Other than that, this treatment method is time consuming and the colour elimination efficiency is unsatisfactory compared to the physical and chemical methods. The initial cost for preparing the large area, such as ponds or a large tank, is very high compared to other methods.

2.3.3   Chemical Treatment

Chemical methods generally utilise reactive oxidative agents to degrade the organic dyes. Advanced oxidation processes (AOPs) are effective oxidation methods to treat textile wastewater.

AOPs involves the formation of radicals, mainly OH radicals from water, to degrade organic pollutants (Chandran, 2015). The OH radicals will attack the chromophores of dye to decolourise them. The degradation of these organic pollutants will produce carbon dioxide (CO_2) and water (H_2O). The products are harmless compared to the physical treatment methods. Ozonation and photochemical oxidation methods are considered as AOPs. Ozonation can oxidise aromatic rings that are found in some dyes due to the strong oxidising power of ozone. Ozonation of chromophores that have conjugated double bonds will produce toxic products. Although prolonged oxidation with ozone can eventually remove these toxic products, it is still undesirable since it is time consuming and requires a larger amount of ozone (Saini, 2017). The main drawback of ozonation is that the gaseous oxidizing agent is very hazardous to human. This implies that the treatment of wastewater with ozone must occur in an enclosed space and be quarantined from the external environment. Therefore, the use of ozone for oxidation must be handled with care to ensure the safety of the handlers.

Photocatalytic degradation is also one of the AOPs. The photocatalytic degradation requires the use of an ultra-violet (UV) light source and photocatalysts to be added for the formation of oxidizing agents. The addition of hydrogen peroxide, H_2O_2 can further increase the generation of hydroxyl (OH) radicals in the wastewater to increase the efficiency of degradation. The efficiency of photocatalytic degradation is affected by a few parameters such as solution pH, types of dye, UV radiation intensity, and the initial dye concentration (Saini, 2017). The photocatalytic

degradation is favoured since it does not produce any toxic products that need to be treated again.

Sonocatalytic degradation uses ultrasound and sonocatalysts to generate radicals for the degradation of organic pollutants. Sonocatalytic degradation provides a better alternative method to treat organic dyes. Based on Zhang, et al. (2011), the penetration of light into the dye wastewater would be decreased since the colours would opaque and hinder the photocatalyst from absorbing the light. For this type of case, sonocatalytic degradation is implemented since the light is not shone from an external environment but generated within the solution. Therefore, sonocatalytic degradation has been investigated to treat textile wastewater.

2.4   Ultrasound Theory

Ultrasound is the interaction between energy and matter (Suslick, 1990). Ultrasound will cause the generation of acoustic bubbles in a solution which enhances the chemical reactions (Gong and Hart, 1998). By concentrating the diffuse energy of sound, cavitation will occur (Suslick, 1990). The occurrence of acoustic cavitation starts with the nucleation of bubbles, followed by the growth, and then ending with the collapse of these bubbles. Upon collapse, hot spots will be generated and sonoluminescence (SL) will be emitted (Qiu, et al., 2018). Formation of cavities in a liquid is known as cavitation. When sound passes through a liquid, it consists of negative-pressure waves and positive-pressure waves. Expansion caused by the negative-pressure, while compression is caused by the positive-pressure during the motion required in the production of cavities (Suslick, 1986). The changes in pressure mark the initiation of sonochemistry. At low-pressure cycle, the bubbles are formed by the diffusion of air molecules into the solution. At high-pressure cycle, the bubble experiences violent compression due to the high external pressure (Pokhrel, Vabbina and Pala, 2016). Thus, the changes in pressure cause the formation of bubbles and the expansion and compression motion. These motions also cause pre-existing bubbles to grow and recompress (Suslick, 1986). The bubble collapses when the external pressure dominates caused by the back and forth motion of the pressure generated by the ultrasound (Pokhrel, Vabbina and Pala, 2016).

The gas phase in the bubble will be at high pressures and temperatures and it will be released when the bubble collapse. The generated pressure and temperature are on the order of hundreds and thousands compared to the operating conditions (Gong

and Hart, 1998). The cavitation implosion will result in a temperature of ~5000 K and a pressure of ~1000 bar (Bang and Suslick, 2010). This sudden explosion of pressure and temperature emits a light that has very short lifetimes (Suslick, 1990). The release of light during collapse of the bubble is known as sonoluminescence (Pokhrel, Vabbina and Pala, 2016). The high release of pressure and energy causes the formation of highly reactive free radicals (Gong and Hart, 1998).

The formation of free radicals occurs at two different spots in the acoustic bubble. Before the oscillating bubble collapse, it can be distinguished into two regions. The two regions are the hot spot region and the surfial region. Figure 2.1 provides a better illustration of the two regions in a bubble. The core will be the part that has the highest temperature.
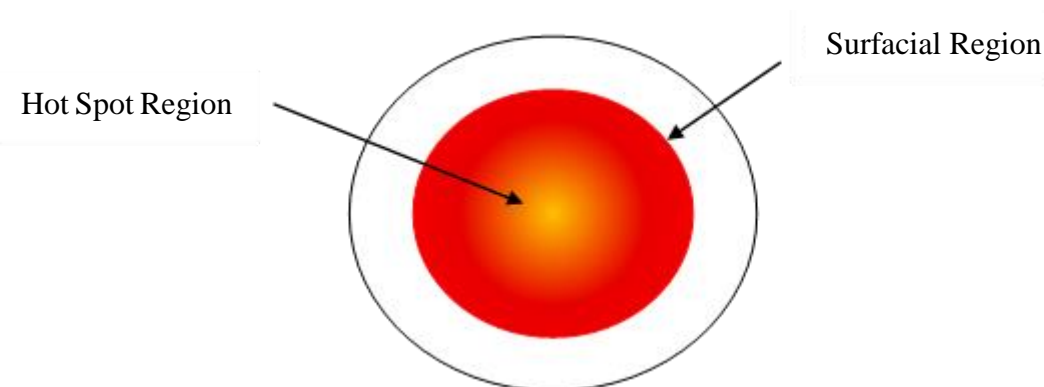
Figure 2.1: The Different Domain Inside an Acoustic Bubble (Pokhrel, Vabbina and Pala, 2016)

The hot spot region is a hot, optically opaque plasma core that results from the compression action by the oscillating bubble (Flannigan and Suslick, 2005). The hot spot region is also known as the gas-phase reaction site (Suslick, 1990). This is because the chemical reaction occurs inside bubble in vapor phase (Pokhrel, Vabbina and Pala, 2016). The surfacial region can also be called as the liquid-phase reaction site (Suslick, 1990). For this region, the chemical reaction initiates outside the bubble in the liquid phase. The radicals formed in the hot spot region are extraordinary radicals while the radicals produced in the surfacial region are ordinary radicals (Pokhrel, Vabbina and Pala, 2016). The difference in types of radicals are caused by the difference in temperature in those two regions. According to Suslick 1990, the initial temperatures are ~5000 K and ~2000 K for the hot spot and surfacial region respectively.

2.5   Heterogenous Sonocatalysis

For sonolysis reaction, the presence of catalyst is favoured. Although the formation of radicals in the liquid body can be done solely by acoustic cavitation, almost all applications requires the presence of a sonocatalyst. This is because ultrasonic irradiation that operates solely by acoustic cavitation is time consuming and requires a large amount of energy. The addition of semiconductor as sonocatalyst can increase the rate of the degradation process which can help to overcome the shortcoming of ultrasonic degradation (Khataee, et al., 2015). The formation of radicals through sonochemistry and sonoluminescence are shown in Figure 2.2. There are two different pathways that produces radicals with the addition of sonocatalyst.
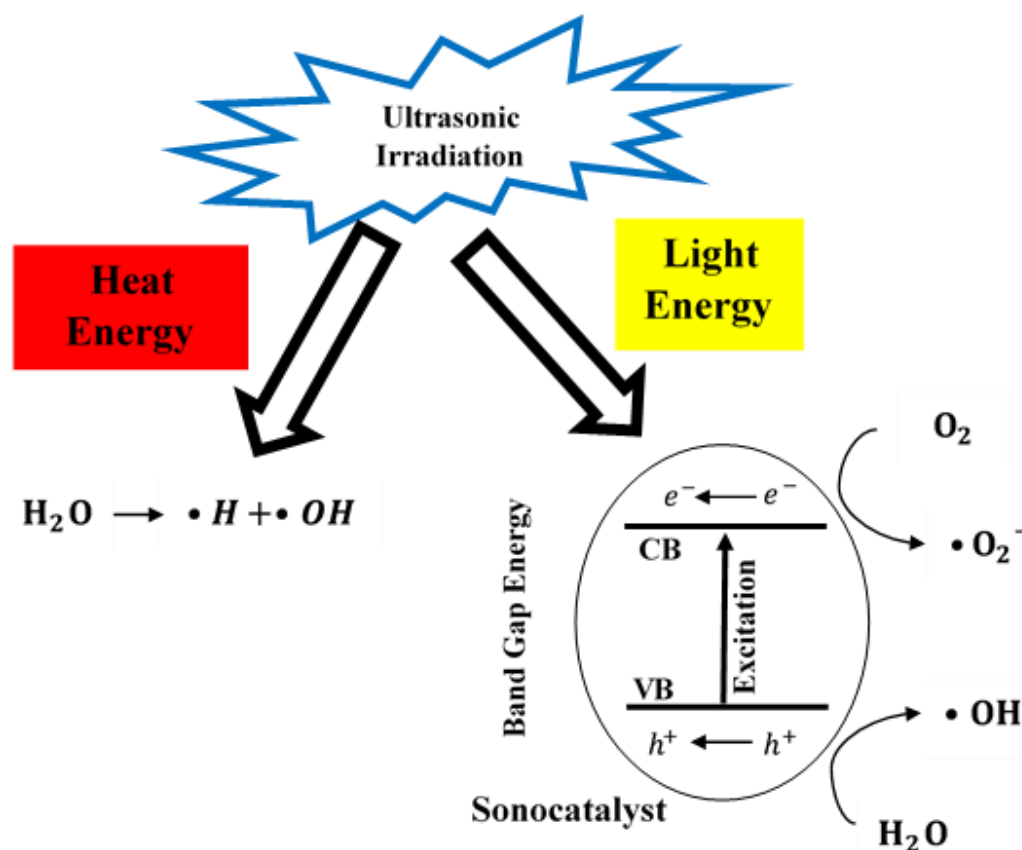
Figure 2.2: The Sonocatalytic Degradation Mechanism in Water (Li, et al., 2018)

There are three mechanisms that will greatly affect the sonocatalytic performance as shown in Figure 2.3. These mechanisms are the heterogeneous nucleation mechanism, photocatalytic mechanism, and thermal catalytic mechanisms. The heterogeneous nucleation will cause more bubbles to nucleate since the presence

of solid surface will lower the surface free energy that is required. Khataee, et al. (2014) stated that the use of a solid sonocatalyst would reduce the energy required for acoustic cavitation because it could provide additional active sites for nucleation of bubbles. The generation of more acoustic bubbles would increase the sonocatalytic activity. The photocatalytic mechanism is caused by the sonoluminescence. The emitted light during bubble collapse has a wavelength of 200 to 700 nm which can excite the electrons in the valence band (VB) of the semiconductor to the conduction band (CB) to generate further free radicals (Qiu, et al., 2018). According to Suslick (1990), the SL spectrum of H_2O peaks at 310 nm and has a broad spectral range throughout the visible light. The third mechanism is the thermal catalytic mechanism. The high temperature condition that occurs during the collapse of bubble will excite the semiconductor thermally. The excitation of semiconductors thermally caused the generation of electron-hole pairs that will lead to the formation of radicals (Qiu, et al., 2018).
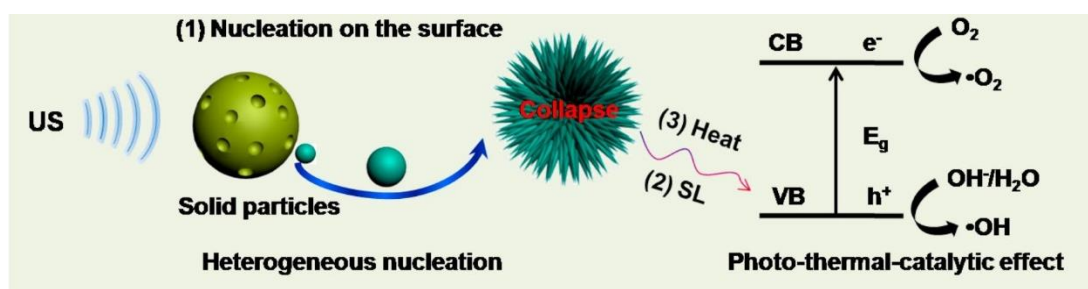
Figure 2.3: Heterogeneous Nucleation, Photocatalytic, and Thermal Catalytic Mechanisms that will Occur in the Presence of a Sonocatalyst (Qiu, et al., 2018)

The formation of radicals that are dependent solely on the acoustic cavitation action has a series of chemical reactions. The chemical equations are listed as Equations (2.1) to (2.5) (Karaca, et al., 2016).

$$H_2O +))) \rightarrow \bullet OH + H \bullet \qquad (2.1)$$

$$\bullet OH + \bullet OH \rightarrow H_2O_2 \qquad (2.2)$$

$$H_2O_2 +))) \rightarrow 2 \bullet OH \qquad (2.3)$$

$$H_2O_2 + \ H \bullet \rightarrow H_2O + \bullet OH \tag{2.4}$$

$$\bullet OH + H \bullet \rightarrow \ H_2O \tag{2.5}$$
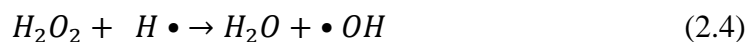
The chemical reactions are due to the sonolysis of water caused by the ultrasound irradiation. The radicals produced can be used to degrade organic pollutants that are present in the water. If the degradation of organic pollutants are solely depended on the radicals formed by the sonolysis of water, the process is unable to perform large-scale treatment of wastewater due to the production of small amount of free radicals (Li, et al., 2018). This leads to the use of photocatalysts in the degradation of organic pollutants by sonochemistry.

In the presence of light and heat, the electrons in the VB of semiconductor can be excited to its CB and it will leave the holes at the VB (Zaman, et al., 2017). In the VB, holes (h^+) would take participation in oxidation reactions on the catalyst surface with the water molecules adsorbed on it. Reduction reactions occurs due to the electrons (e^-) in conduction bond reacting with dissolved O_2 to generate radicals (Dehghan, Kakavandi and Kalantary, 2018). The processes are illustrated by Equations (2.6) to (2.8).

$$Sonocatalyst + \ ))) \ \rightarrow \ e^- + \ h^+ \tag{2.6}$$

$$e^- + \ O_2 \rightarrow \ O_2^- \bullet \tag{2.7}$$

$$h^+ + \ H_2O \rightarrow \bullet OH \tag{2.8}$$
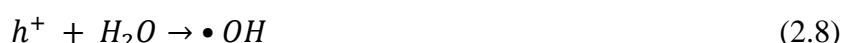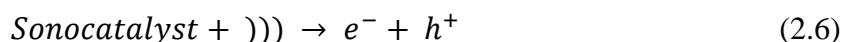
The radicals formed by the three mechanisms in a sonocatalytic process can be utilized for degradation of organic matters. The reaction is shown in Equation (2.9).

$$\bullet OH/O_2^- \bullet/H \bullet \ + Organic \ matter \ \rightarrow \ CO_2 + \ H_2O \tag{2.9}$$

2.6   Sonocatalysts

There are many types of sonocatalysts that can be used for removing organic dye pollutants. The two most popular sonocatalysts used are TiO_2 and zinc oxide (ZnO). The favouritism for these two metal oxides are due to their exceptional optical, ,

chemical and physical properties, non-toxicity, low cost, and complete mineralization. (Nuengmatcha, et al., 2016) The band-gap energy of TiO_2 is 3.2 eV. TiO_2 will be activated when an ultraviolet light with wavelength shorter than 380 nm is present. This will cause the formation of radicals which able to degrade the organic matter in water (Zhu, et al., 2013). Since the SL from the ultrasound irradiation emits a light with wavelengths from 200 to 800 nm, this proves that titanium dioxide is suitable for this application. However. There are some limitations and drawbacks for both TiO_2 and ZnO. The disadvantages of using pure TiO_2 are the relatively high intrinsic band gap energy of TiO_2 and high rate of electron-hole recombination of the generated photo-holes and photo-electrons (Nuengmatcha, et al., 2016). The limitations for pure ZnO semiconductors are the rapid recombination rate of electron–hole pairs and low-charge separation efficiency (Ong, Ng and Mohammad, 2018).

The main drawbacks of these two common sonocatalysts are the large band gap energy that reduced the utilisation of the light in the visible region. The implementation of a non-metal sonocatalyst known as graphitic carbon nitride ($g-C_3N_4$) will provide a smaller band gap energy compared to these two sonocatalysts. The cost of $g-C_3N_4$ synthesis is lower than the TiO_2 and ZnO since it has various synthesis pathways and the raw materials can be found abundantly. The cheaper and metal-free sonocatalyst shows great potential to be implemented as a sonocatalyst.

2.7   Graphitic Carbon Nitride ($g-C_3N_4$)

$G-C_3N_4$ is a metal-free catalyst that has a medium band gap structure which shows potential in formation of radicals in water (Dong, et al., 2014). Since this catalyst is found abundantly, it will be cheaper compared to the other metal-based catalysts. $G-C_3N_4$ has a tunable electronic structure, excellent chemical stability and a unique 2D-structure (Zhao, Sun and Dong, 2014). There are seven predicted phases for $g-C_3N_4$, every one of them will have different band gap energy level. This proves that the $g-C_3N_4$ has a tunable electronic structure. The seven different phases are cubic C_3N_4, pseudocubic C_3N_4, α-C_3N_4, g-otriazine, g-h-triazine, β-C_3N_4, and g-h-heptazine which have band gap energy level of around 4.3 eV, 4.13 eV, 5.5 eV, 0.93 eV, 2.97 eV, 4.85 eV and 2.88 eV respectively (Wang, et al., 2017). The $g-C_3N_4$ with the phase of g-h-heptazine is mainly focused due to the small band gap energy that has the potential of water splitting efficiency. The main drawback of pure $g-C_3N_4$ is the rapid recombination of electron-hole pairs. With the rapid recombination, the catalytic

activity for g-C$_3$N$_4$ is lowered (Zhao, Sun and Dong, 2014). Other than that, g-C$_3$N$_4$ has lower surface area compared to the metal catalysts which causes the number of active sites for interfacial reactions to decrease and it also has a low charge (Wang, et al., 2017).

G-C$_3$N$_4$ has a band gap that is narrower than TiO$_2$ and ZnO. The band gap energy for g-C$_3$N$_4$ is around 2.7 eV. With such a low band gap, the absorption spectra of this catalyst can go up to the visible light region without any doping (Xu, et al., 2015). The polymeric properties also allow it to have high chemical stability. The structure of g-C$_3$N$_4$ is similar to graphite where the π-conjugated planes of g-C$_3$N$_4$ are made up of C and N atoms linked together through sp^2 hybridization. The π-bonds between the planes indicates that the g-C$_3$N$_4$ are linked together by covalent bonds. S-triazine and tri-s-triazine, also known as s-heptazine, are the basic structures of g-C$_3$N$_4$ (Xu, et al., 2015). Both s-triazine and s-heptazine does not have C-C and C-H bonds, making them both special cases of N-heterocycles. S-triazine and s-heptazine are nitrogen rich rings having molecular formula of C$_3$N$_3$ and C$_6$N$_7$ respectively. The molecular structure of both rings are shown in Figure 2.4. With the absence of C-C and C-H bonds, the g-C$_3$N$_4$ has a high thermal and oxidative stability. This is because the structure is made up of C-N bonds that have high bond dissociation energies which require tremendous energy to break up these bonds. Oxidative stability is achieved due to the high electronegativity of nitrogen that will enhance the oxidation number of carbon (Makowski, 2012).
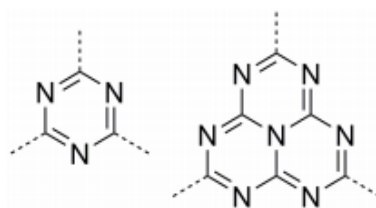
Figure 2.4: Molecular Structure of S-triazine (left) and S-heptazine (right) (Makowski, 2012)

Full structure of g-C$_3$N$_4$ is illustrated in Figure 2.5. The most stable allotrope among all phases of g-C$_3$N$_4$ is the phase that is constructed by s-heptazine units. It has very high stability at ambient conditions (Dong, et al., 2014). The unique structure without of C-C and C-H bonds, g-C$_3$N$_4$ can withstand up to 600 ^{O}C in air. By heating the g-C$_3$N$_4$ until 550 ^{O}C, it will cause an increase in band gap energy and surface area.

This is because the high heat treatment will exfoliate the structure of g-C_3N_4. To further prove that g-C_3N_4 is a versatile material, the crystalline structure can become amorphous and red if heated in Argon to a temperature of 600 ^{O}C (Sun, et al., 2018). G-C_3N_4 has been found to dissociate to nitrogen and cyano fragments when heated beyond 700 ^{O}C (Wang, et al., 2017). This implies that if it is heated above this temperature, the g-C_3N_4 will lose its unique structure and its functionality since all the bonds are already broken.
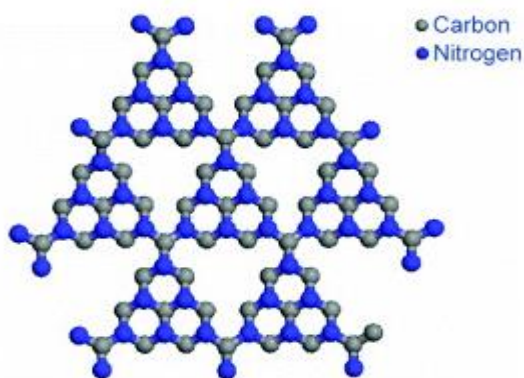
Figure 2.5: The Molecular Structure of g-C_3N_4 (Yue, et al., 2011)

As seen in Figure 2.5, the lattice structure is similar to graphene's. The main difference between graphene and g-C_3N_4 is the presence of nitrogen atoms that are partially substituted in the carbon lattice. The nitrogen atoms in the g-C_3N_4 mostly exist as graphitic and pyridinic nitrogen (Wang, et al., 2017). G-C_3N_4 is a n-type semiconductor, which means that there is a large number of free electrons that act as mobile carriers. The nitrogen atoms in the planar g-C_3N_4 act as donors easily by losing their excess electron to contribute the free electron in the structure (Fang, et al., 2015). The unique planar structure of g-C_3N_4 is made up of graphitic and pyridinic nitrogen to exhibit high thermal stability, versatility and free moving electrons, which cause it to be an interesting catalyst that has high potential for improvement.

As mentioned before, g-C_3N_4 has a tunable band structure that makes it more promising as a catalyst. With this characteristic, the catalyst has a wide range of applications. The flexible property provides two major advantage to g-C_3N_4. The first advantage is the VB and CB of the catalyst can be controlled to obtain the optimum band gap energy to increase the activity and efficiency of the catalyst. Secondly, the

adjustable electronic structure will allow heterojunctions and elemental doping to be easier since the structure modification process to couple with other semiconductors can be simplified (Dong, et al., 2014). Figure 2.6 shows the predicted band structure of g-C_3N_4 and pure TiO_2 at pH=7. The highest occupied molecular orbitals (HOMO) of the s-heptazine are derived from the nitrogen p_z orbitals. The combination of these orbitals make up the VB of g-C_3N_4 while the CB is the combination of the lowest unoccupied molecular orbitals (LUMO). The LUMO for g-C_3N_4 is derived from the carbon p_z orbitals (Sun, et al., 2018). The nitrogen and carbon p_z orbitals make up the VB and CB respectively. Based on Figure 2.6, the LUMO of CB from g-C_3N_4 is positioned at around -1.3 V. This shows that the CB of g-C_3Ns_4 has a more negative value compared to the reduction of CO_2, the evolution of H_2, and the reduction reactions of O_2. G-C_3N_4 can easily reduce smaller molecules such as CO_2, O_2 and H_2O due to the large thermodynamic driving force that is caused by the sufficient difference in negativity between the molecules and the CB (Wang, et al., 2017). The reduction of water is very important to form hydrogen radicals that will degrade the organic pollutants. The HOMO of the VB is located around 1.4 V which is quite low compared to the VB of TiO_2. The smaller value causes the VB to have a smaller thermodynamic driving force to oxidise water molecules for the degradation of organic pollutants. The performance of g-C_3N_4 on water oxidation and degradation of organic pollutants can be improved by decreasing the position of VB to enhance the oxidation strength of g-C_3N_4 (Chu, et al., 2013).

There are many ways to enhance the catalytic properties of g-C_3N_4, the most common way is by doping it with metal oxide or non-metal ions such as TiO_2 or carbons. In general, the doping of metal ions will allow the absorption of visible light since it will further lower the band gap energy of g-C_3N_4 (Dong, et al., 2014). According to Tripathi and Narayanan (2018), the photocatalytic efficiency of TiO_2/g-C_3N_4 was higher than pure TiO_2 by 10 % and more. This showed that the doping of metal oxide on the g-C_3N_4 could enhance the ability to degrade organic pollutants. The doping with non-metal ions would also increase the catalytic efficiency of g-C_3N_4.
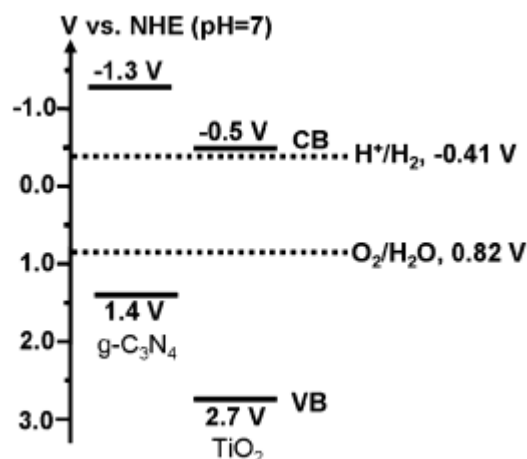
Figure 2.6: The Band Structure of G-C₃N₄ and TiO₂ (Chu, et al., 2013)

Besides, heterojunctions structure with g-C$_3$N$_4$ could also decrease the recombination rate of electron and hole pairs by separating them effectively (Dong, et al., 2014). The offset between the two structures must be enough to allow effective migration for the electrons and holes. Otherwise, the electrons and holes will easily undergo recombination, rendering the heterojunctions useless. Dong, et al. (2014) has stated that the separation and transfer of electrons and holes between g-C$_3$N$_4$ and cadmium sulphide (CdS) is very effective due to the well-matched overlapping band structures. By combining these two materials, the catalytic activity can be increased and the self-oxidation of CdS can be prevented since the holes will be transferred to g-C$_3$N$_4$. Another example of heterojunction is the isotype heterojunction with the combination of thiourea g-C$_3$N$_4$ (CN-T) and urea g-C$_3$N$_4$ (CN-U) as shown in Figure 2.7. The CB of these two materials have an offset of 0.10 eV while the VB has an offset of 0.40 eV. The heterojunction can stabilize the electrons and holes by keeping the electrons at the CN-U side while the holes at the CN-T side. The separated electrons and holes would prevent them from recombining and increase the catalytic efficiency. The heterojunction can also prolong the lifetime of charge carriers which will result in the increased production of radicals (Zhao, Sun and Dong, 2014). The distribution of electrons to one side and holes to the other will make the catalyst more efficient because it will remove the recombination potential of the electron and hole pair.
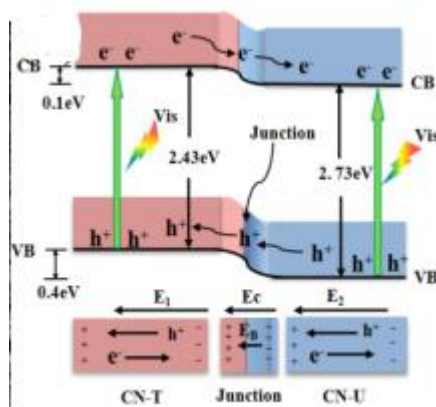
Figure 2.7: Band Structure of CN-T/CN-U (Zhao, Sun and Dong, 2014)

Heterostructures can greatly enhance the catalytic activity by migrating the charges to either sides in the composite structure. The separation of charges will restrain the recombination of the electron and holes which will boost up the formation of radicals for degradation of organic pollutants (Dong, et al., 2014).

2.8   Carbon

With the trend moving toward a more sustainable technology, the incorporation of carbon with sonocatalyst are greatly increased. The incorporation of carbon materials with sonocatalysts provides the most attractive possibilities since the addition of carbon materials allows the combination of adsorptivity and sonocatalytic activity (Toyoda, et al., 2016). According to López-pe, et al. (2013), the addition of carbon materials will improve the sonocatalyst physically and chemically. For the improvement of physical properties, carbon materials will increase the surface area of the sonocatalyst due to its porous structure. This will increase the contact surface area between the pollutant in the solution and the sonocatalyst incorporated with carbon materials. Other than that, the increased surface area with the addition of carbon materials can provide more catalytic sites for the sonocatalytic degradation process. The increase in number of catalytic sites will produce more free radicals which will increase the sonocatalytic performance of the sonocatalyst. The carbon material can also act as a support for the sonocatalyst to increase the strength of fragile sonocatalysts. For the affect of carbon material on the chemical property, it was found out that carbon materials exhibit impressive sonocatalytic performance by themselves. The large surface area will increase the formation of acoustic bubbles due to heterogeneous nucleation (Khataee, et al., 2014). The increased formation of acoustic

bubbles will cause more free radicals to be generated which further increases the sonocatalytic degradation efficiency of the sonocatalyst.

The incorporation of carbon material to sonocatalyst can also cause the sonocatalyst to have better charge separation. The rapid recombination rate of electron-hole pairs always poses a problem for sonocatalysts since the rapid recombination will reduce the production of free radicals. Carbon materials will act as the electron collector and transporter which delays the recombination rate of electron-hole pairs (Marie, et al., 2019). The characteristic of carbon that have good adsorption capacity can also help improve the performance of sonocatalyst. With the target pollutant adsorbed on the catalyst surface, the degradation of the pollutants can be done more efficiently. This is due to the relatively short lifetime of OH radicals. If the pollutants are adsorbed on the catalyst surface, most of the OH radicals generated can tackle the molecules and degrade them.

The incorporation of carbon material with sonocatalyst can improve the sonocatalytic performance by increasing the surface area, delaying the recombination rate of electron-hole pairs, increasing the generation of acoustic bubbles, and having good adsorption capacity.

2.9   Carbon Quantum Dots (CQDs)

CQDs is also known as carbon nanodots (CNDs) or carbon dots (C-dots) (Wang, et al., 2017). CQDs is widely used to enhance the catalytic activity because it can up-convert photoluminescence (UCPL), which means it can increase the range of spectra absorption. CQDs also have high aqueous solubility and can prevent the recombination of electron and holes in the catalyst (Hong, et al., 2016). CQDs differs from normal carbon dopants in particle size where CQDs are smaller than 10 nm. CQDs are quasi-spherical carbon nanoparticles that has a structure that is amorphous to nanocrystalline with the presence of carbon atoms bonded in the form of graphene-type sp^2 hybridization and diamond-type sp^3 hybridization (Wang, et al., 2017)

The utilization of CQDs as a dopant for catalytic activity will greatly improve the activity and efficiency of the catalyst. Doping CQDs can bring about three major advantages. The first advantage is that CQDs will enlarge the range of the absorption spectra. This means that a larger portion of the solar radiation can be harvested and used to increase the number of excited electrons. CQDs themselves have VB and CB to form electrons and holes. These electrons are excited by the light spectrum that falls

in the UV and near-visible region (Makama, Umar and Saidu, 2018). The electrons in the CB of CQDs can transfer to the CB of the doped semiconductor or used to increase the production of radicals. According to Wang, et al. (2017), CQDs that are excited can show promising electron transfer properties. This statement further proves the fact that the excited electrons from CQD can be transferred to the semiconductor. The second characteristic of CQD that can cause the semiconductor to absorb a wider range of light spectra is the UCPL properties. UCPL is an optical phenomenon that converts light with longer wavelength to light with shorter wavelength (Makama, Umar and Saidu, 2018). With this property, the catalyst can be excited even when the wavelength of light is longer than the absorption region because the wavelength of light will be shortened by CQDs. CQDs can also cause the semiconductor's band gap to be narrower due to the bonding between them that will result in broadening of light spectra absorption (Makama, Umar and Saidu, 2018). The second advantage of doping CQDs is that it enhances charge separation. CQDs can improve the quantum efficiency of semiconductors that has a more negative LUMO by accepting their excited electrons to prevent the recombination of the electron-hole pairs. This can be achieved since CQDs has a strong electron affinity and an intrinsic band gap (Makama, Umar and Saidu, 2018). The prevention of charge recombination will greatly improve the quantum efficiency of the doped catalyst. Lastly, doped CQDs can increase the surface area for adsorption and reaction. Since CQDs is a nano-sized particle with size less than 10 nm, it will naturally possess a large surface to volume ratio. The more adsorption surface area will result in an increased chance of the target reactants to react which enhances catalytic activity (Makama, Umar and Saidu, 2018).

2.10 Characterisation of pure g-C_3N_4 and Carbon/g-C_3N_4 Composites

The characterisation of heterogenous catalyst is an important study since it will provide information that can allow us to understand the synthesised catalyst better. There are various methods that can be used to characterise g-C_3N_4. The catalyst g-C_3N_4 could be characterised by using X-Ray diffraction (XRD), scanning electron microscopy-Energy dispersive X-ray (SEM-EDX) and Fourier-transform infrared (FTIR).

XRD plays a major role in characterisation because it can analyse and provide structural properties of the sample at an atomic scale. XRD uses X-ray beams that are generated from cathode ray tubes to form monochromatic beams after filtration. As the incident X-ray comes in contact with an atom, the electrons will oscillate and cause

constructive and destructive interferences. Destructive interferences are the combination of waves that are out of phase which will not be detected by the detector in XRD. The wave that are in phase will interact constructively and a well-defined X-ray will leave the sample and be detected by the detector (Bunaciu, Udriştioiu and Aboul-Enein, 2015). XRD is very capable in determining the relative abundance of crystalline compounds that are present in a heterogeneous solid mixture. The identification of components present in the sample is based on the fingerprints of every element, which is the diffraction data, that is stored in the International Centre for Diffraction Data. Other than that, XRD can also characterise the crystallographic structure and provide an estimation of crystallite sizes based on the Scherrer Equation. There are a few limitations for XRD analysis. The sample must exhibit crystalline structure or else no result will be detected. The analysis of samples at high angles will cause peaks to overlap and provide inaccurate results. Niu, et al. (2018) reported that the g-C_3N_4 catalyst will have diffraction peaks at 13.2^O and 27.3^O.

The topography image can be obtained by using SEM. SEM-EDX analysis can be used to provide compositional and morphological information (Choudhary and Priyanka, 2017). SEM can provide the surface image of the specimen since it utilises a beam of high energy electrons to strike of the sample. The principle is similar to light microscopy where the light is substituted with electron beams. The electron beams will travel to the sample in a vacuum region and is directed and focused by electromagnetic lenses and metal apertures. Once the electron beam strikes the surface of the sample, various types of electrons will be formed. The electrons formed are backscattered electron, secondary electrons, auger electrons, X-rays, and cathodoluminescence. The backscattered and secondary electrons will provide the topography related information while the auger electron and X-ray displayed compositional information. The main drawbacks of SEM are the image formed will only be black and white since electron beams are used as the light source and it can only detect samples that are solid, inorganic and small enough to be placed on the specimen holder (Choudhary and Priyanka, 2017). The only difference between SEM and SEM-EDX is the addition of EDX. EDX is a technique that can analyse the composition by determining the relative abundance of elements that are present on the surface of the specimen (Olea-Mejia, et al., 2014). By detecting the X-rays that will be produced when the sample is being struck by the electron beam, the difference in energy detected in the X-ray can provide the compositional information of the specimen. Only X-rays produced by atoms with

atomic numbers greater than four can be detected (Olea-Mejia, et al., 2014). In short, the implementation of SEM-EDX can provide topographical, morphological and even composition information about g-C_3N_4 and the dopant present for better understanding.

FTIR analysis can identify the chemical groups present in the sample by probing the vibrational properties of the chemical bonds present in the sample. FTIR can give complementary information to the results obtained from XRD (Berthomieu and Hienerwadel, 2009). When infrared radiation is passed through a sample, the sample with chemical bonds will absorb the IR radiation at a specific frequency (Bunaciu, Aboul-Enein and Fleschin, 2010). The frequency of absorption differs with the types of bonding that are present in the molecular system. This difference in frequency absorption allows FTIR to detect specific compounds that are present in the specimen. The combination with the mathematical fourier transform for IR spectroscopy allows quantitative and qualitative information to be obtained rapidly (Bunaciu, Aboul-Enein and Fleschin, 2010). Since g-C_3N_4 has a molecular structure that consists of C and N atoms that are double and single bonded, the application of FTIR is useful to identify the types of species present and the way they are bonded with each other. Based on Qin and Zeng (2017), the bending and stretching vibration of C – H bonds are seen at peaks of 1404 cm^{-1} and 2924 cm^{-1} respectively. C = C and C $\equiv$ C bonds will have characteristic absorption at 1625 cm^{-1} and 2360 cm^{-1} respectively. For g-C_3N_4, the stretching mode of the CN heterocycles will be displayed by peaks at 1325 cm^{-1}, 1439 cm^{-1}, 1575 cm^{-1}, and 1639 cm^{-1}. The bending modes of the s-triazine units can be seen at 806 cm^{-1} while the broad peak at 3180 cm^{-1} shows the stretching vibration of N – H groups (Marcì and Palmisano, 2018).

2.11   Parameter Studies

There are several parameters that can affect sonocatalytic activity. The types of dyes, catalyst dosage, amount of carbon, hydrogen peroxide (H_2O_2) dosage, solution pH and initial dye concentration will be studied.

2.11.1   Effect of Carbon Amount

The concentration of carbon composited will affect the degradation efficiency of the sonocatalyst. Pure g-C_3N_4 has low surface area and a rapid recombination rate between the electron-hole pairs. The incorporation of g-C_3N_4 with carbon can increase the degradation efficiency of the sonocatalyst since carbon can eliminate these two limitations of pure g-C_3N_4. According to Marie, et al. (2019), the carbon composite
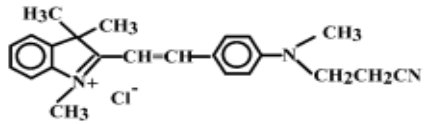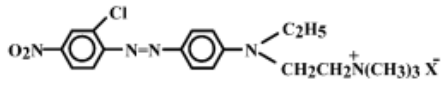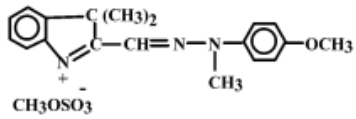
would provide more catalytic sites since it has a large surface area. The composition of carbon could also delay the recombination rate of the electron-hole pairs which increases the generation of free radicals in the solution for better degradation performance. s

2.11.2   Effect of Ultrasonic Irradiation on Different Dyes

Textile wastewater usually consists of various types of dyes. It is predicted that different types of dye will experience different degradation rates since they differ in molecular structure. Lorimer, et al. (2001) reported that Basic Red 18 has the fastest degradation rate followed by Basic Yellow 28 with Basic Red 14 degrading the slowest. These three types of dyes are decolourised at constant conditions of ultrasonic frequency of 510 kHz and ultrasonic power of 1.1 W/cm^2. The difference in molecular weight and types of bonds present will affect the degradation of that specific dye. OH radicals will have higher reactivity with the class of dye that has azo dyes present (Abdullah and Pang, 2010). Table 2.4 illustrates the physical properties of these three different dyes for better comparison.

Based on the molecular structures, the presence on azo dyes (-N=N-) can only be seen in Basic Red 18 dye. The degradation rate for this dye was reported to be the fastest among three types of dyes. Therefore, the presence of azo dyes will greatly increase the degradation rate when ultrasonic irradiation is used. The Basic Yellow 28 degrades faster than Basic Red 14. The higher molecular weight of Basic Yellow 28 implies that it has a larger molecule structure. In summary, the presence of azo bond and a larger molecular structure would allow the dyes to be degraded easily under ultrasonic irradiation.

Table 2.4: Molecular Structure and Molecular Weight of Different Dyes (Lorimer, et al., 2001)

Name of Dye	Molecular Weight	Molecular Structure
Basic Red 14	379.93	
Basic Red 18	426.34	
Basic Yellow 28	433.52	

2.11.3 Effect of Hydrogen Peroxide (H_2O_2) Dosage

H_2O_2 is very useful in sonocatalytic processes because it is a very strong oxidizing agent. The presence of H_2O_2 can produce more OH radicals via two routes. The first route is by reducing the H_2O_2 at the CB of the respective sonocatalyst present (Abbasi and Asl, 2008). According to Farhadi and Siadatnasab (2016), H_2O_2 will produce OH radicals that will be responsible for the degradation of organic pollutants by reacting with the electrons found in the CB of sonocatalysts. H_2O_2 can also increase the generation of OH radicals through self-decomposition that is induced by ultrasound irritation. The self-decomposition is shown in Equation 2.10.

$$H_2O_2 +))) \rightarrow 2 \bullet OH \tag{2.10}$$

Farhadi and Siadatnasab (2016) reported that the degradation efficiency of Methylene Blue was only 15 % in the absence of H_2O_2. As the dosage of H_2O_2 was raised from 10 to 30 mmol/L, the degradation of the organic pollutant had increased from 39 % to 100 %. This was most likely caused by the generation of OH radicals from H_2O_2. When the dosage of H_2O_2 was more than 30 mmol/L, the was no increase in degradation efficiency.

Although H_2O_2 can greatly increase the degradation efficiency of the sonocatalytic system, over dosage of the oxidizing agent can also reduce the efficiency

of the system. Abbasi and Asl (2008) stated that excessive dosage of H_2O_2 would cause less pollutants to be degraded because the oxidizing agents around would act as a scavenger of OH radicals and VB holes. Similarly, Pang and Abdullah (2012) also stated that H_2O_2 would undergo a self-quenching process of OH radicals if they are present in high concentrations. This process would produce hydroperoxyl radicals (OOH•) which have much lower oxidation potential as compared to OH radicals. The formation of the OOH radicals is shown in Equation 2.11.

$$H_2O_2 + \bullet\, OH \;\rightarrow\; H_2O + \bullet\, OOH \tag{2.11}$$

Other than reducing the amount of OH radicals present in the system, the high concentration of H_2O_2 can also increase the toxicity of the wastewater (Purswani, et al., 2014). If too much H_2O_2 is added, the toxicity of the wastewater effluent will increase. This is undesirable since the treated wastewater should be less toxic than it is before treatment. Purswani, et al. (2014) recommended a maximum concentration of 1 g/L of H_2O_2. Higher concentration would be very risky since it might bring more hazards when it is discharged to environment. Therefore, the optimum concentration of H_2O_2 should be determined to prevent excessive dosage of H_2O_2 in the wastewater solution.

2.12   Optimisation Study

The optimisation study will be done by using the Design Expert 11. The response surface methodology (RSM) will be used for the optimisation study. The implementation of this method provides easy and accurate statistical tools for the analysis and design of experiments. The RSM can determine the optimum operating conditions of the studied factors to achieve best results at a minimal cost (Stat-Ease, 2018). Without the implementation of RSM, the relationship between the studied independent variables and the response factor will not be known.

The Central Composite Design (CCD) model will be chosen as the template for the RSM. The CCD model can generate an empirical relationship between the independent variables by obtaining a small fraction of results from a full three-level factorial. There are three types of point considered by the CCD model which are factorial, axial, and centre points. The CCD template requires the repetitive run for the centre points, ideally six times of repetition. The experiments should be conducted

randomly to obtain better results for the model (Stat-Ease, 2018). The three independent variables that will be used for the CCD modelling are initial dye concentration, initial catalyst loading, and solution pH. The effect of these parameters on the response factor, which is the degradation efficiency of organic dye, are discussed.

2.12.1 Effect of Initial Dye Concentration

The composition of textile wastewater effluent will vary for every discharge. This will affect the dye concentration that is present in the wastewater. The change in concentration will affect the degradation efficiency. Based on Song, et al. (2012), the initial pollutant concentration would greatly affect the degradation efficiency. It was reported that the efficiency would drop from 89 % to 67 % when the initial MB concentration was increased from 5 to 20 mg/L.

The decrease in efficiency was due to the insufficient amount of OH radicals generated. Since other parameters were remained constant, the presence of higher concentration of organic pollutant will not change the amount of oxidative agent produced. If the amount of OH radicals remained constant, the increase in dye concentration would cause a decrease in degradation efficiency (Song, et al., 2012). Other than that, the increased amount of dyes would inhibit the degradation by causing interferences for the formation of oxidative agents (Abbasi and Asl, 2008).

2.12.2 Effect of Catalyst Dosage

The dosage of sonocatalyst in the treated solution may affect the degradation rate of organic dyes. The accelerated rate when increasing catalyst dosage is caused by the increased OH radical's production. This is due to an increase in active reaction sites. The additional sonocatalyst in the solution will provide more surface for the nucleation of cavitation bubbles (Farhadi and Siadatnasab, 2016). Song, et al. (2012) reported that the degradation efficiency of increased as the dosage of the sonocatalyst increased. The efficiency increased from 48 % to 96 % as the g-C_3N_4 dosage raised from 0.5 to 2.0 g/L. The generation of OH radicals will increase with the increased amount of sonocatalyst in the solution. This concludes that the efficiency will increase as more sonocatalyst is present in the wastewater solution.

This linear relation applies until a certain limit is reached. At higher catalyst dosage, the sonocatalysts will aggregate and decrease the efficiency in degradation of

the targeted pollutants. The aggregation causes effective surface area to be reduced which leads to a decrease in number of active sites to produce OH radicals. Other than that, the excessive amount of sonocatalyst in the solution will reduce the amount of cavitation bubbles formed because they will hinder the circulation of ultrasonic waves (Farhadi and Siadatnasab, 2016). Thus, the optimum catalyst dosage shall be the one where the degradation efficiency is the highest at the lowest catalyst dosage.

2.12.3   Effect of Solution pH

Solution pH of the textile wastewater can contribute greatly to the degradation efficiency of the organic dyes present. Pang and Abdullah (2012) stated that solution pH would affect the surface binding-sites of the catalyst and also the chemical form of reactants in the sample. He, et al. (2018) reported that OH radicals would transformed back into water at solution pH 2. At acidic condition, hydrogen ions (H^+) will scavenge OH radicals and convert them back into water, causing a decrease in oxidation of the organic pollutants as shown in Equation 2.12.

$$H^+ + \bullet OH + e^- \rightarrow H_2O \qquad (2.12)$$

Heymann, et al. (2018) had reported the effects of solution pH on g-C_3N_4 and Methylene Blue. The adsorption of Methylene Blue was found to be lower at low solution pH values while it was higher at a high solution pH level. This implied that the adsorption of the targeted pollutants will be better at a more alkaline solution. It was also reported that the rate constant for the degradation of organic pollutants in increased at alkaline condition. This makes sense since a higher adsorption rate would allow more organic pollutants to be degraded.

2.13   Reusability Study

This study shows the durability of the sonocatalyst. The durability is important to determine the lifespan of a catalyst. A reusable catalyst has more value since it does not need to be replaced after every operation. This could reduce the operating cost and save the environment by reducing the waste contributed by the catalysts. Sonocatalysts might experience a change in size and structure when irradiated by ultrasound waves. Therefore, this study is crucial to determine whether the sonocatalyst can withstand the ultrasound power and continue to provide similar degradation efficiency.

The test for reusability of the sonocatalyst can be done by operating the same catalyst for a few cycles. The degradation efficiency of each cycle is determined to check if there is deterioration. If the efficiency dropped as the cycles increases, the sonocatalyst was said to be not that stable for the degradation of organic pollutants under ultrasonic irradiation (Farhadi and Siadatnasab, 2016).

2.14   Summary of Chapter 2

This chapter contains the literature review done for this report. Since the target pollutant for this report is organic dye, the classification of dyes and the basis for colour of dyes are discussed. The available textile wastewater treatment methods were studied. This report focused on the sonocatalytic degradation of pure g-C_3N_4, pure carbon, and carbon/g-C_3N_4 composite at different weight percentage. The theory behind sonocatalysis and the properties of the pure and incorporated samples were also discussed. The theoretical effect of various parameters on the degradation efficiency was also researched along with the implementation of Design Expert 11.

CHAPTER 3

METHODOLOGY AND WORK PLAN

3.1   Materials and Chemicals
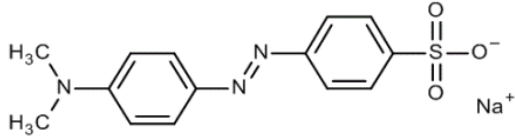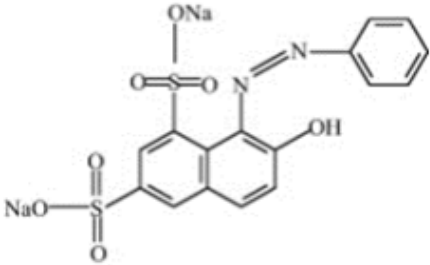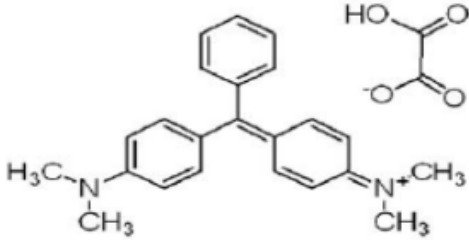
The raw materials that are required to synthesise the sonocatalyst are tabulated in Table 3.1. For the synthesis of g-C_3N_4, urea was used as the raw material. H_2O_2 was added into the solution to act as oxidising agent to increase the degradation of organic dye. Three types of organic dyes were chosen for treatment, which are Methyl Orange, Acid Orange G, and Malachite Green.

Table 3.1: Name, Purity, Brand and Uses of Chemical Reagent Used

Chemical Reagents	Purity	Brand	Uses
Urea	-	R&M Chemicals	Catalyst synthesis
Hydrogen Peroxide (H_2O_2)	30 %	SYSTHERM	Oxidising agent
Sodium Hydroxide (NaOH)	-	R&M Chemicals	Adjustment of pH
Hydrochloric Acid (HCl)	-	Sigma-Aldrich	Adjustment of pH
Acid Orange G	-	Sigma-Aldrich	Organic pollutant
Methyl Orange	-	Fischer Scientific	Organic pollutant
Malachite Green	-	R&M Chemicals	Organic pollutant

This research focused on treating three different organic dyes. The organic dyes that were chosen are the Methyl Orange, Acid Orange G, and Malachite Green. The main reason for selecting these three organic dyes were to identify which dye would be degraded most efficiently by ultrasonic irradiation in the presence of the chosen sonocatalyst. The structures, classifications and molecular weight of these three dyes were displayed in Table 3.2. The difference in molecular weight and type of chromophores could affect the degradation efficiency for the sonocatalyst. The three chosen dyes have different molecular weight and chromophores.

Table 3.2: Chemical Structure, Classification, and Molecular Weight of Model Pollutants

Dye	Classification	Molecular Weight	Chemical Structure
Methyl Orange	Acidic Anionic Azo dye	327.33	
Acid Orange G	Acidic Anionic Azo dye	452.37	
Malachite Green	Basic Cationic Triarylmethane	364.91	

3.2 Equipment

Several equipment and instruments were used for this research. The usage of these equipment was divided into the synthesis of catalyst, characterisation of catalyst, experimental set-up, and liquid sample analysis. The instruments and equipment that were used were shown in Table 3.3. The catalyst samples were prepared by using a furnace. The samples were then characterised by three separate equipment which were namely X-ray diffraction (XRD), scanning electron microscopy-energy dispersive X-ray (SEM-EDX), and fourier-transform infrared (FTIR). The solution pH was measured by using a pH meter. The ultrasonic irradiation was provided by an ultrasonic processor. Syringe filters were implemented to filter out the sonocatalyst from the liquid sample for liquid sample analysis. The concentration of organic dye present was detected by UV-Vis spectrophotometer. The COD of the water sample was measured by the COD machine.

Table 3.3: Model of Equipment Used

Equipment Used	Model
XRD	Shidmazu XRD-6000
FTIR	Nicolet IS10
SEM-EDX	Hitachi S-3400N
Furnace	Nabertherm M41H
pH Meter	Sartorius PB-10
COD Tester	HACH DR3900
Ultrasonic Processor	Hielscher UP400S
UV-Vis Spectrophotometer	CARY 100 Conc

3.3 Overall Experiment Flowchart

The flowchart for this research was shown in Figure 3.1. The carbon was synthesised by pyrolysis of coconut shell husk in a furnace. The preparation of pure g-C_3N_4, pure carbon, and carbon/g-C_3N_4 composite at different weight percentage were carried out. The catalysts prepared were characterised by XRD, SEM-EDX, and FTIR. The parameters that would greatly affect the degradation efficiency were experimented. The parameters that were considered were the different carbon amount, types of organic dyes used, and H_2O_2 dosage. The optimisation study was done by using Design Expert 11 with a Central Composite Design (CCD) Model. The factors that would be included in the study were initial dye concentration, initial catalyst loading, and solution pH. The concentration of organic dye in liquid samples were measured by using the UV-Vis spectrophotometer. COD analysis was also carried out for the liquid sample. The reusability study of the chosen sonocatalyst on the dye degradation were studied.

3.4 Experiment Set-up

Figure 3.2 showed the experimental set-up for the treatment of organic dyes in the ultrasonic bath. The parameters of the ultrasonic bath set at 80 W. The conical flask was filled with the organic dye solution and sample catalysts. The beaker was placed on the stage of the ultrasonic processor and the beaker was lifted up with the stage to allow the ultrasonic processor to come in contact with the solution.

```
┌──────────────┐          ┌────────────────────────┐
│   Carbon     │   ⟹     │  Pure g-C₃N₄ and       │
│  Synthesis   │          │  Carbon/g-C₃N₄ Composite│
│              │          │  at Different Weight    │
└──────────────┘          └────────────────────────┘
```

Carbon Synthesis ⟹ **Pure g-C$_3$N$_4$ and Carbon/g-C$_3$N$_4$ Composite at Different Weight**

⬇

Characterisation of Catalyst
- XRD
- SEM-EDX
- FTIR

⬇

Parameter Studies
- Carbon Amount (1, 5, 10, 15, 20, 25 wt%)
- Types of Organic Dyes (Methyl Orange, Acid Orange G, Malachite Green)
- H$_2$O$_2$ Dosage (0, 0.10, 0.25, 0.50, 1.00, 1.50 mmol/L)

Optimisation Studies
- Initial Dye Concentration (20 to 25 ppm)
- Initial Catalyst Loading (0.3 to 0.5 g/L)
- Solution pH (4 to 8)

⬇   ⬇

Liquid Sample Analysis
- UV-Vis Spectrophotometer
- COD Analysis

Reusability

Figure 3.1: Flowchart for Overall Research Activities
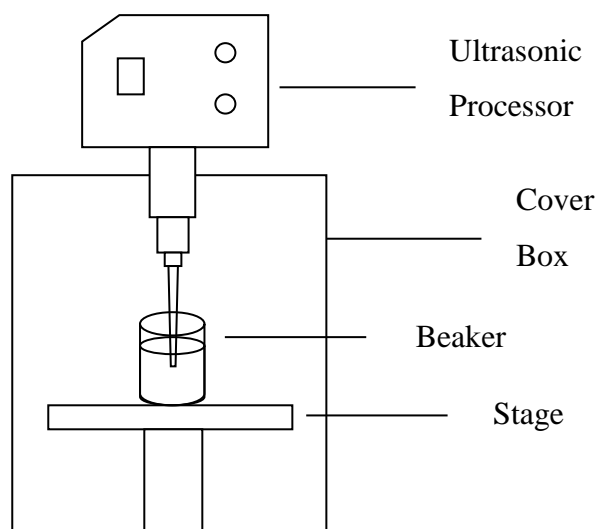
Figure 3.2: The Experimental Set-up

3.5 Experimental Procedures

3.5.1 Preparation of Pure g-C$_3$N$_4$, Pure Carbon, and Carbon/g-C$_3$N$_4$ Composite at Different Weight Percentage

5 g of urea was placed into an open crucible in the muffle where the sample was kept at 500 ^{O}C for 2 hours (Yu, et al., 2018). The g-C$_3$N$_4$ was then grounded into fine powders. The carbon/g-C$_3$N$_4$ composite at different weight percentage were prepared by adding a 0.05 g, 0.25 g, 0.5 g, and 0.75 g, 1.00 g, and 1.25 g of carbon in the urea. The steps for synthesis after the addition remains the same. The obtained products were denoted to be 1 wt% C/g-C$_3$N$_4$, 5 wt% C/g-C$_3$N$_4$, 10 wt% C/g-C$_3$N$_4$, 15 wt% C/g-C$_3$N$_4$, 20 wt% C/g-C$_3$N$_4$, and 25 wt% C/g-C$_3$N$_4$.

3.5.2 Preparation of Carbon from Coconut Shell Husk

The coconut shell husk was left out to dry for 2 days to decrease the moisture of the husk. The dried husk was then carbonised by pyrolysis at 750 ^{O}C for 1 hour. The resulting sample were crushed by using a mortar and pestle to be in powder form. The carbon powder was sieved to a constant size of 100 μm.

3.5.3 Preparation of Organic Dyes

Stock dye solutions from different dyes of 500 mg/L were prepared by mixing 0.5 g of dye powder into deionised water of 1 L. The stock solutions were diluted to obtain the desired concentration that was required.

3.6 Characterisation of Catalysts

Several equipment was used to characterise the catalyst that was prepared. This was a very important step as it will provide some information on the structure of catalyst surface, composition of catalyst, and chemical properties of the catalyst. The characterisation of catalyst could provide explanation to the performance of the catalyst. The equipment that were used in this research were XRD, SEM-EDX and FTIR.

The crystalline composition was found out by using XRD. XRD provided information on the crystalline structure and gave an estimation for the crystallite size. The characterisation of the samples was carried out in Shidmazu Model XRD-6000 using Cu Kα radiation. The X-ray tube were set to the parameters of 25 mA and 45 kV. The prepared samples were scanned from 2θ starting from 10° and ending at 60°.

The SEM-EDX used for this research was the Hitachi S-3400N. This equipment was used to obtain information on the surface structure of the sample. The topological and morphological information could be obtained by implementing this equipment. The addition of EDX gave results on the relative abundance of elements present on the surface of the sample. The scanning voltages used are 5.0 kV.

The FTIR could provide identification on the chemical group present by detecting the bonding between atoms. The peaks that were displayed in the results showed the abundance and presence of a certain chemical bonding. The FTIR used in this research was Nicolet Model IS10.

3.7 Parameter Studies

Different parameters that would affect the degradation efficiency were studied. Some variables must be kept constant during the study of these parameters to isolate out the effect of that specific parameter on the degradation efficiency. The parameters that were kept constant during the experiment were the ultrasound frequency, treatment time, and volume of dye solution. The volume of dye solution was kept at 100 mL before the addition of sonocatalyst into the solution. The treatment time was kept constant at 10 minutes for every sample. The ultrasound frequency that irradiated the sample has an output power of 80 W. The initial and final dye concentration were measured by a UV-Vis spectrophotometer. The results were used for the calculation for degradation of dye.

3.7.1 Effect of Carbon Amount

The effect of different weight percentage of carbon composited with g-C_3N_4 was first analysed. The different weight percentage of carbon that were prepared were 1 wt%, 5 wt%, 10 wt%, 15 wt%, 20 wt%, and 25 wt% which were denoted to be 1 wt% C/g-C_3N_4, 5 wt% C/g-C_3N_4, 10 wt% C/g-C_3N_4, 15 wt% C/g-C_3N_4, 20 wt% C/g-C_3N_4, and 25 wt% C/g-C_3N_4. The remaining parameters were set at a constant value of initial dye concentration at 15 ppm, 0.3 g/L initial catalyst loading, and natural solution pH. The organic dye chosen for treatment is Malachite Green. The catalyst that has the best degradation efficiency was used for the subsequent studies.

3.7.2 Effect of Ultrasonic Irradiation on Different Dyes

The effect of different types of organic dyes that were treated were carried out by comparing three different dyes. The Methyl Orange, Acid Orange G, and Malachite Green were treated separately to obtain the degradation efficiency for each dye. The parameters that were yet to be determined are the solution pH, initial dye concentration, and initial catalyst loading. These parameters were set at natural solution pH, 15 ppm, and 0.3 g/L, respectively. The dye that provided the best degradation efficiency was carried forward and used in the subsequent studies.

3.7.3 Effect of H_2O_2 Dosage

Under similar ultrasonic irradiation, the effect of different H_2O_2 dosage was found out. The concentration of H_2O_2 was varied between five values which are 0 mmol/L, 0.10 mmol/L, 0.25 mmol/L, 0.50 mmol/L, 1.0 mmol/L and 1.50 mmol/L. The initial dye concentration was kept at 15 ppm while the catalyst loading was 0.3 g/L. The type of organic dye treated was determined in the previous experiment. The optimum H_2O_2 dosage that was determined is brought forward for the subsequent studies.

3.8 Design of Expert (DoE)

The interactive relationships between the three factors that would affect the degradation efficiency of Malachite Green was studied by using DoE. The three significant factors were initial dye concentration (X_1), initial catalyst dosage (X_2), and solution pH (X_3). The response factor to be optimised was the degradation efficiency of Malachite Green. With the three parameters being manipulated, the other factors were remained constant. The other factors were the chosen catalyst with the best

degradation efficiency, the type of organic dye selected, H_2O_2 dosage, and 100 mL of dye solution.

The Response Surface Methodology (RSM) was implemented with the use of a Central Composite Design (CCD) model. The DoE was done by using Design Expert 11. With three factors being the manipulated variables, a total of 20 experimental runs were required for the CCD model. The calculation method was shown in Equation 3.1.

$$Total\ Number\ of\ Runs = 2^n + 2n + 6 \qquad (3.1)$$

where
n = number of variables

The first and second term of Equation 3.1 represented the number of factorial points and axial points needed to run experimentally. The last term indicated the centre points of the CCD model. The axial points were located at ± 1.682 from the centre point. The coded and actual range of values for the three parameters were displayed in Table 3.4

Table 3.4: Actual and Coded Values for the Three Variables Used in CCD

Variables	Factors	Actual Values for the Coded Levels				
		-α (-1.682)	-1	0	+1	+α (+1.682)
Initial Dye Concentration (ppm)	X_1	18.30	20.00	22.50	25.00	26.70
Initial Catalyst Loading (g/L)	X_2	0.232	0.300	0.400	0.500	0.568
Solution pH	X_3	2.6	4.0	6.0	8.0	9.4

The point types, run numbers, and experimental conditions with their respective actual and coded values were tabulated in Table 3.5. The data in Table 3.5 were generated by CCD using Design Expert 11. The experiments were conducted for 10 minutes with an output power of 80 W for the ultrasonic processor. The degradation efficiency of Malachite Green for each run was obtained after 10 minutes for results comparison to determine the interactive effects.

Table 3.5: Experiment Matrix of CCD

Standard Order	Point Type	Coded Independent Variable Levels		
		Initial Dye Concentration, ppm (X_1)	Initial Catalyst Loading, g/L (X_2)	Solution pH (X_3)
1	Factorial	20.00 (-1)	0.300 (-1)	4.0 (-1)
2	Factorial	25.00 (+1)	0.300 (-1)	4.0 (-1)
3	Factorial	20.00 (-1)	0.500 (+1)	4.0 (-1)
4	Factorial	25.00 (+1)	0.500 (+1)	4.0 (-1)
5	Factorial	20.00 (-1)	0.300 (-1)	8.0 (+1)
6	Factorial	25.00 (+1)	0.300 (-1)	8.0 (+1)
7	Factorial	20.00 (-1)	0.500 (+1)	8.0 (+1)
8	Factorial	25.00 (+1)	0.500 (+1)	8.0 (+1)
9	Axial	18.30 (-1.682)	0.400 (0)	6.0 (0)
10	Axial	26.70 (+1.682)	0.400 (0)	6.0 (0)
11	Axial	22.50 (0)	0.232 (-1.682)	6.0 (0)
12	Axial	22.50 (0)	0.568 (+1.682)	6.0 (0)
13	Axial	22.50 (0)	0.400 (0)	2.6 (-1.682)
14	Axial	22.50 (0)	0.400 (0)	9.4 (+1.682)
15	Centre	22.50 (0)	0.400 (0)	6.0 (0)
16	Centre	22.50 (0)	0.400 (0)	6.0 (0)
17	Centre	22.50 (0)	0.400 (0)	6.0 (0)
18	Centre	22.50 (0)	0.400 (0)	6.0 (0)
19	Centre	22.50 (0)	0.400 (0)	6.0 (0)
20	Centre	22.50 (0)	0.400 (0)	6.0 (0)

3.9 Reusability Study

The used 10 wt% C/g-C_3N_4 was centrifuged at 10,000 rpm for 30 minutes to separate the used catalyst from the degraded solution. After centrifuging, the catalyst was cleaned by rinsing with distilled water and collected on a filter paper. It was then oven dried for 3 hours at a temperature of 80 °C. The catalyst was then reused to degrade a new batch of Malachite Green solution.

3.10   Liquid Sample Analysis

The liquid samples were analysed by using UV-Vis spectrophotometer and COD tester. UV-Vis spectrophotometer was used to detect the initial and final concentration of organic dye in the liquid sample. A calibration curve of absorbance against concentration was plotted to determine the organic dye concentration. The absorbance was expected to be directly proportional to the concentration according to the Beer-Lambert Law. By testing the liquid sample, the concentrations were obtained, and the degradation efficiency was calculated. The degradation efficiency of any system can be calculated out by using Equation 3.2.

$$Degradation\ efficiency = \left(1 - \frac{C_0}{C_t}\right) \times 100\ \% \qquad (3.2)$$

where

C_0 = initial dye concentration, mg/L

C_t = dye concentration at time t, mg/L

The COD analysis was also applied to determine the initial and final COD of the liquid sample. The COD for the samples were obtained by using a COD tester. The COD value was good indicators of water quality.

3.11   Summary of Chapter 3

This chapter consists of the materials, chemicals, and equipment used for the experiment conducted. A flowchart and experimental set up was also included in this chapter. The experimental matrix for the optimisation study from Design Expert 11 is also shown here. The procedure for reusability study and experimental work for various parameters was shown. The calculation of degradation efficiency was shown.

CHAPTER 4

RESULTS AND DISCUSSION

4.1   Characterisations of Pure g-C$_3$N$_4$, Pure Carbon, and Carbon/g-C$_3$N$_4$ Composite at Different Weight Percentages

The characterisations of pure graphitic carbon nitride (g-C$_3$N$_4$), pure carbon, and carbon/g-C$_3$N$_4$ composite at different weight percentages were performed by using X-ray diffraction (XRD), scanning electron microscopy-energy dispersive X-ray (SEM-EDX), and fourier-transform infrared (FTIR) analysis. By analysing the samples, the difference between pure g-C$_3$N$_4$, pure carbon, and carbon/g-C$_3$N$_4$ composite at different weight percentage could be observed.

4.1.1   X-ray Diffraction Analysis

The XRD results for pure g-C$_3$N$_4$, pure carbon, and carbon/g-C$_3$N$_4$ composite at different weight percentages are shown in Figure 4.1. By analysing the pure g-C$_3$N$_4$ peak, it was observed that there was no peak at 13.1° but three other peaks at 27.5°, 37.9°, and 44.1° appeared in by the XRD pattern. The characteristic peaks for pure g-C$_3$N$_4$ were located around 13.1° and 27.5° (An, et al., 2017). The (002) interlayer stacking peak of graphitic layered material, which is the conjugated aromatic system, is represented by the peak of 27.5° while the peak at 13.1° corresponds to (100) in-plane repeated s-triazine units (An, et al., 2017). Although there was no peak at 13.1°, the peak at 27.5° confirmed the presence of the layered structure of carbon nitride which proves that the catalyst produced was indeed g-C$_3$N$_4$. Meanwhile, the peak at 44.1° represented the crystallography plane of g-C$_3$N$_4$ at (020) (Tyborski, et al., 2013).

As carbon is composited with g-C$_3$N$_4$, the peak at 27.5° became smaller. With the amount of carbon composited with g-C$_3$N$_4$ increasing, the peak was diminished and eventually disappeared when carbon amount was set at 10 wt %. The diminishing of peak at 27.5° was caused by a disorder in the in-plane repeated packing brought upon by the composited carbon (Zhang, et al., 2019). This implied that carbon composited with the g-C$_3$N$_4$ structure caused a decrease in the ordered structure or the interlayer stacking (An, et al., 2017). For g-C$_3$N$_4$ with carbon weightage above 15 wt%, all the characteristic peaks of g-C$_3$N$_4$ were lost from the XRD analysis. The disappearance of g-C$_3$N$_4$ peaks were due to the presence of excessive amount of carbon

in the sample. As the amount of carbon increased from 15 wt%, the characteristic peaks of pure carbon appeared as shown in the XRD pattern for 25 wt% C/g-C$_3$N$_4$. The emergence of peaks at 28.3° and 40.4° for the sample with a carbon of 25 wt% indicates that carbon was dominating the sample. The broad peak shown for 15 wt% C/g-C$_3$N$_4$ and 20 wt% C/g-C$_3$N$_4$ were caused by the high amount of amorphous carbon material.

The XRD pattern for pure carbon showed two significant peaks which are at 28.3° and 40.4° respectively. The amorphous carbon-based material were hemicellulose, amorphous cellulose, and lignin (Rout and Singh, 2011). The peak shown at the diffraction angle of 40.4° showed the (100) crystallography plane of carbon (Taer, et al., 2018). According to Rout, et al. (2016), the pyrolyzed coconut shell also showed a peak around 28.3° which reinforced the implication that the carbon produced was indeed carbon.
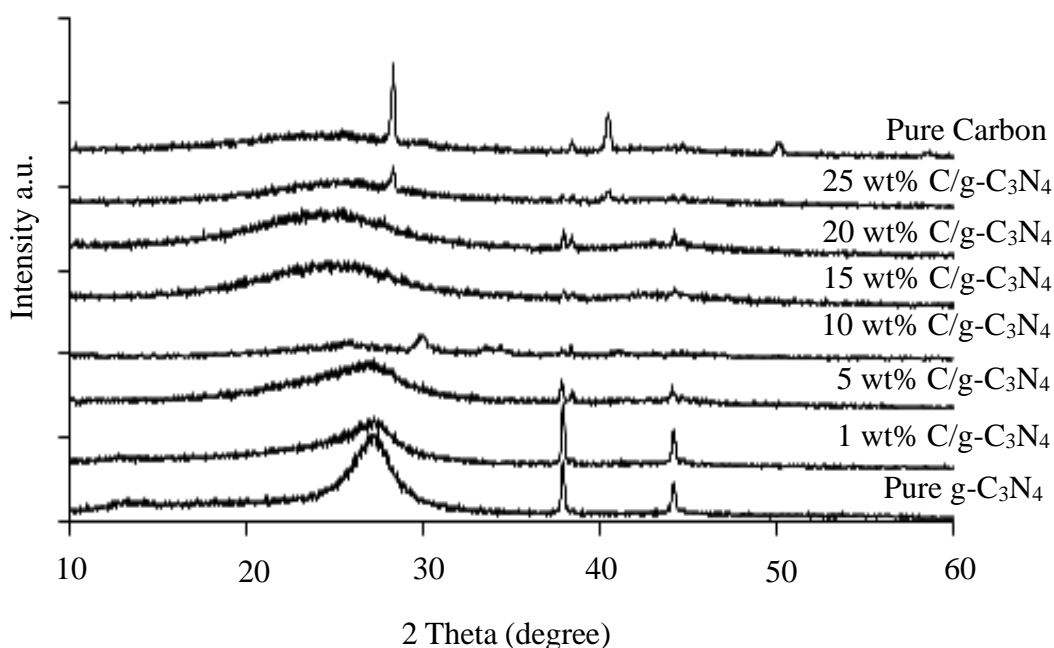
Figure 4.1: XRD Patterns of Pure g-C$_3$N$_4$, Pure Carbon, and Carbon/g-C$_3$N$_4$ Composite at Different Weight Percentages

4.1.2 Scanning Electron Microscopy-Energy Dispersive X-ray Analysis

Figure 4.2 illustrates the surface morphology of pure g-C$_3$N$_4$, pure carbon, and carbon/g-C$_3$N$_4$ composite at different weight percentages at a 5,000 magnification. Figure 4.2 (a) shows that pure g-C$_3$N$_4$ has a structure that resembles overlapping flat sheets with irregular shape and irregular porous. This was consistent with the finding

reported by Yue, et al. (2016). Figure 4.2 (b) shows the SEM image for 1 wt% C/g-C_3N_4 samples and consist of smoother surface with the irregular shapes. This implied that the smoother surface was the carbon material. Figure 4.2 (c) displayed that the smoother surface was becoming more dominant rather than the irregular shapes that was seen in the pure g-C_3N_4.

The SEM image of 10 wt% C/g-C_3N_4 shown in Figure 4.2 (d) revealed that fewer irregular shapes, which indicated the dominance of the carbon materials over g-C_3N_4. The SEM images reflected the results obtained from XRD where the characteristic peaks of g-C_3N_4 were diminished and eventually disappeared as the amount of carbon increased. As the amount of carbon increased, the presence of the irregular shaped particles decreased as shown in Figure 4.2 (e), Figure 4.2 (f), and Figure 4.2 (g) which were represented by carbon amount of 15 wt%, 20 wt%, and 25 wt%, respectively. The decrease in the irregularly-shaped particles implied that there is a decrease in g-C_3N_4 on the carbon material. This is caused by the increased amount of carbon material which increased the surface area of the sample. The distribution of g-C_3N_4 were more spread-out with an increased surface area which explained the the decreasing amount of g-C_3N_4 on the carbon material. Figure 4.2 (h) shows the SEM image for pure carbon. The image indicated that there were signs of cracks and residues on the carbon material with no irregular shaped particles present.

The EDX results with the weightage of carbon and nitrogen elements are shown in Table 4.1. Pure g-C_3N_4 showed the carbon to nitrogen ratio of 0.78 which was very close to the stoichiometric carbon to nitrogen ratio which had a value of 0.75. The introduction of carbon material to the pure g-C_3N_4 catalyst caused a rapid increase in carbon weightage. As the carbon materials increased up to 5 wt%, the carbon element detected by EDX was capped at a range of 85 wt% to 90 wt%. This implied that the 5 wt % carbon was enough to completely fill the surface of g-C_3N_4. The EDX results showed that the pure carbon had a 2.15 wt% of nitrogen. The minor amount of nitrogen present in the sample was due to the pyrolysis in the presence of air.
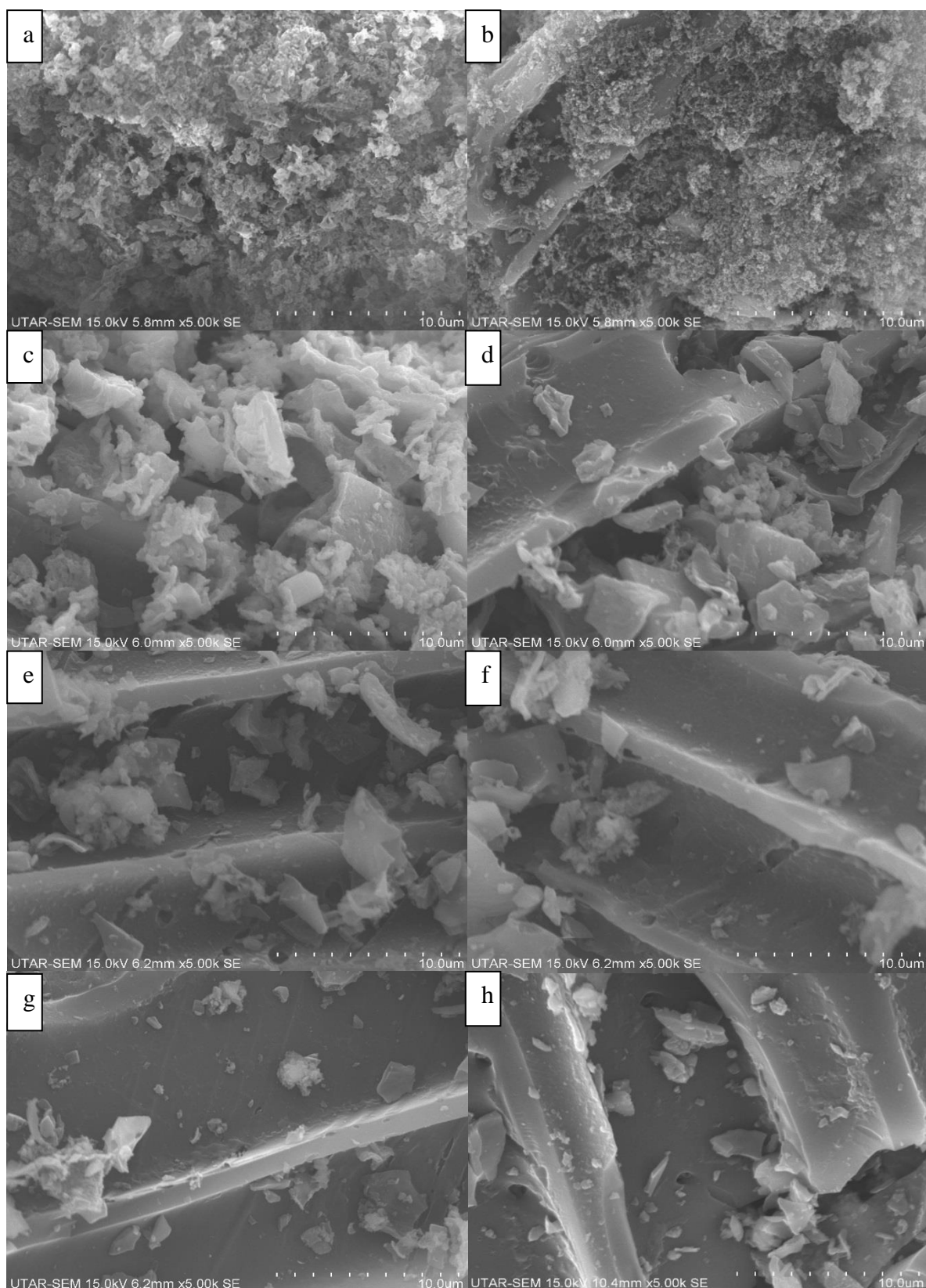
Figure 4.2: SEM Images of (a) Pure g-C₃N₄ (b) 1% C/g-C₃N₄ (c) 5% C/g-C₃N₄ (d) 10% C/g-C₃N₄ (e) 15% C/g-C₃N₄ (f) 20% C/g-C₃N₄ (g) 25% C/g-C₃N₄ (h) Pure Carbon

Table 4.1: EDX Results for Pure g-C₃N₄, Pure Carbon, and Carbon/g-C₃N₄ Composite at Different Weight Percentage

Samples	C		N	
	Wt %	At %	Wt %	At %
Pure g-C₃N₄	43.81	47.62	56.19	52.38
1 wt% C/g-C₃N₄	49.12	52.96	50.88	47.04
5 wt% C/g-C₃N₄	85.31	87.14	14.69	12.86
10 wt% C/g-C₃N₄	87.42	89.01	12.58	10.99
15 wt% C/g-C₃N₄	88.22	89.72	11.78	10.28
20 wt% C/g-C₃N₄	86.30	88.02	13.70	11.98
25 wt% C/g-C₃N₄	89.72	91.06	10.28	8.94
Pure Carbon	97.85	98.15	2.15	1.85

4.1.3 Fourier-Transform Infrared Analysis

The results from the FTIR analysis for pure g-C$_3$N$_4$, pure carbon, and carbon/g-C$_3$N$_4$ composite at different weight percentages are shown in Figure 4.3. The FTIR band for pure g-C$_3$N$_4$ showed a broad weak band at 3170.2 cm^{-1}. According to Liu, et al. (2011), the broad weak band located at 3235.9 cm^{-1} indicated the stretching vibration modes for the N − H groups. Other than the broad peak, intense bands were observed at 1541.5 cm^{-1}, 1508.1 cm^{-1}, 1458.4 cm^{-1}, and 1400.1 cm^{-1}. The results indicated that there were heptazine-derived repeating units in the sample since they were the typical stretching vibration modes of these units (Liu, et al., 2011). There were also well-defined peaks at 1239.2 cm^{-1} and 805.6 cm^{-1}. The peak observed at 1239.2 cm^{-1} represented the presence of C-NH-C groups in the sample. The peak was resulted from the incomplete polymerisation of the heptazine units (Thurston, et al., 2017). The out-of-plane bending vibration characteristic of heptazine rings was represented by the peak observed at 805.6 cm^{-1} (Liu, et al., 2011).

With the addition of carbon as composite, the peaks observed in pure g-C$_3$N$_4$ became less distinctive. The intense bands found from 1550 cm^{-1} to 1400 cm^{-1} were lost in 1 wt% C/g-C$_3$N$_4$ with peaks only showing at 1559.9 cm^{-1} and 1406.5 cm^{-1}. For 5 wt% C/g-C$_3$N$_4$ and 10 wt% C/g-C$_3$N$_4$, both samples showed that the peaks at 1239.2

cm^{-1} and 805.6 cm^{-1} were lost. The intense bands that were observed in pure g-C$_3$N$_4$ were also found to be less for the samples. This implied that the composition of carbon with g-C$_3$N$_4$ would make g-C$_3$N$_4$ lose its characteristics by hindering the formation of the repeating heptazine units. The FTIR results for 15 wt% C/g-C$_3$N$_4$, 20 wt% C/g-C$_3$N$_4$, and 25 wt% C/g-C$_3$N$_4$ were observed to be similar to the FTIR results of pure carbon. This indicated that the composition of excess carbon with g-C$_3$N$_4$ would cause the g-C$_3$N$_4$ to completely lose its characteristics.

For the FTIR result for pure carbon, no distinct peaks were observed from 4000 cm^{-1} to 400 cm^{-1}. The result obtained was found to be the same with the result reported by Li, Ha and Kim (2009). This indicated that the pure carbon synthesised were single wall carbon tubes.
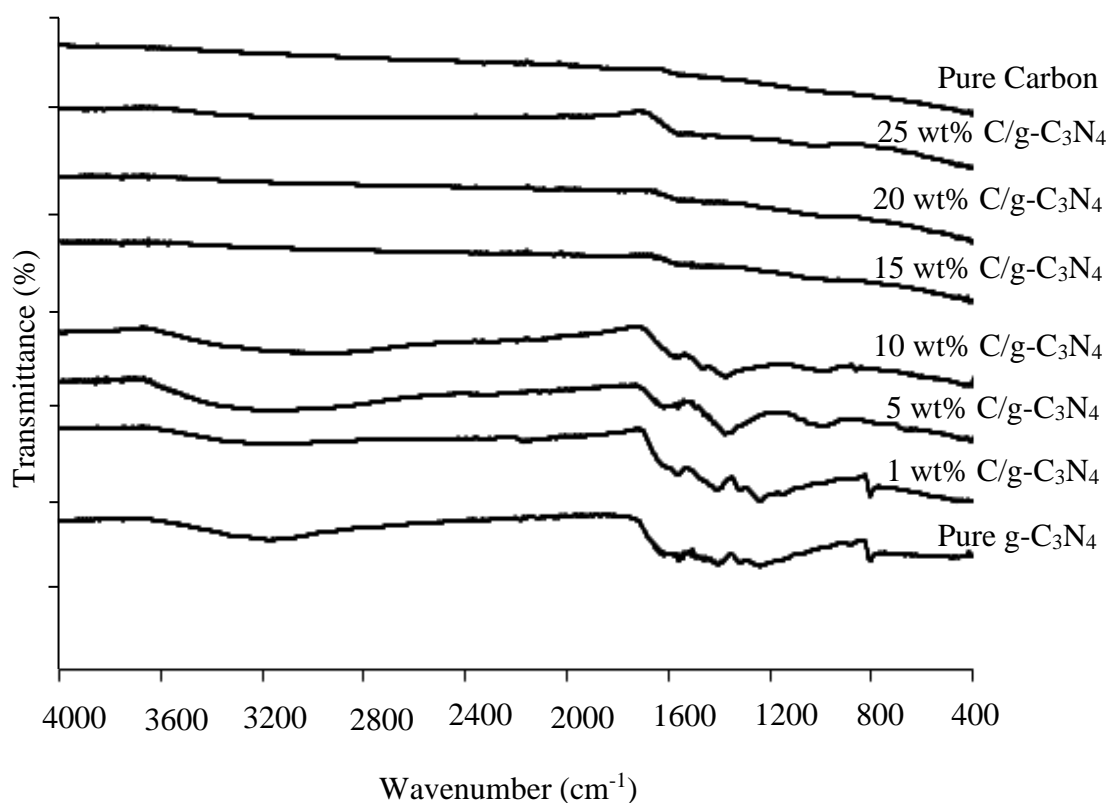
Figure 4.3: FTIR Results of Pure g-C$_3$N$_4$, Pure Carbon, and Carbon/g-C$_3$N$_4$ Composite at Different Weight Percentages

4.2   Parameter Studies in Sonocatalytic Process

4.2.1   Effect of Carbon Amount Composited with g-C₃N₄

The effect of different carbon amount composited with $g\text{-}C_3N_4$ is studied by comparing the degradation efficiencies of Malachite Green which are shown in Figure 4.4. Figure 4.4 shows that $g\text{-}C_3N_4$ that is composited with 10 wt % of carbon showed the best degradation efficiency of 93.44 %. Pure $g\text{-}C_3N_4$ only shows the lowest degradation efficiency of 11.20 %. The 10 % $C/g\text{-}C_3N_4$ provided around 8 times better degradation efficiency of Malachite Green as compared to the pure $g\text{-}C_3N_4$. The degradation efficiency of $g\text{-}C_3N_4$ composited with carbon showed an increment results until maximum degradation efficiency was achieved. The degradation efficiencies for 1 wt% $C/g\text{-}C_3N_4$ and 5 wt% $C/g\text{-}C_3N_4$ were 18.23 % and 57.93 %, respectively. After the optimum degradation efficiency was reached, the further addition of carbon amount on $g\text{-}C_3N_4$ showed a decrement result. The degradation efficiencies for 15 wt% $C/g\text{-}C_3N_4$, 20 wt% $C/g\text{-}C_3N_4$, and 25 wt% $C/g\text{-}C_3N_4$ were 86.08 %, 87.96 %, and 83.28 %, respectively. Meanwhile, the degradation efficiency of Malachite Green in the present of pure carbon was only 67.17 %.
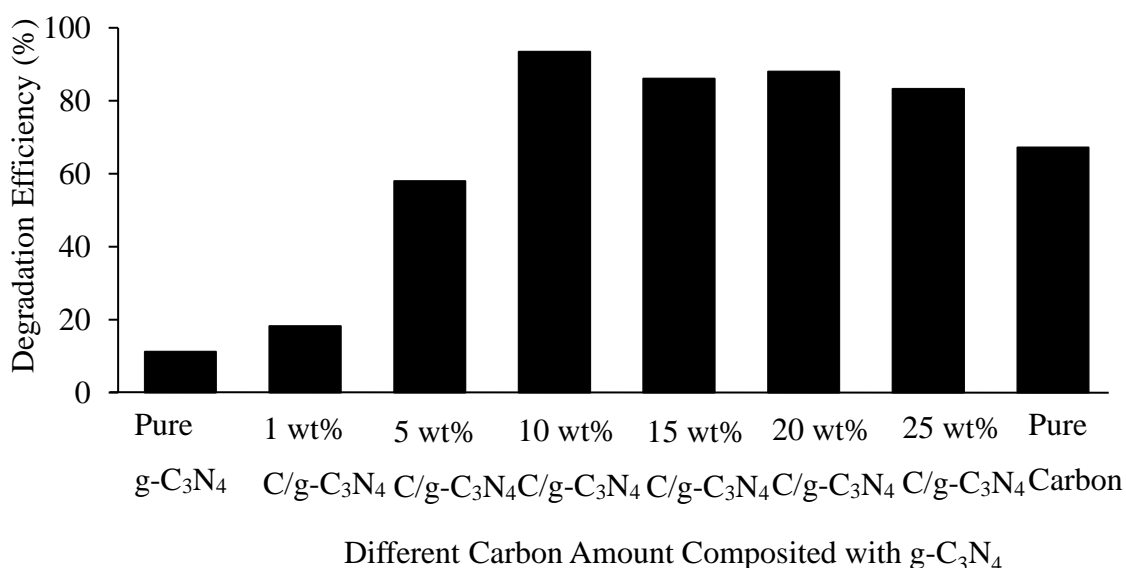
Figure 4.4: Degradation Efficiency of Different Carbon Amount Composited with g-C₃N₄ (Initial Malachite Green Concentration = 15 ppm, Initial Catalyst Loading = 0.3 g/L, and Natural Solution pH for 10 Minutes)

Pure g-C$_3$N$_4$ showed a very poor catalytic performance due to low surface area and rapid recombination rate of the electron-hole pairs (Zhao, Sun and Dong, 2014). The carbon and g-C$_3$N$_4$ composite could improve the catalytic performance in many ways. The large surface area of composite sample could provide more catalytic sites for the sonocatalytic degradation process. The compositing of carbon could also help to delay the recombination rate of electron-hole pairs because carbon could serve as the electron collector and transporter. By allowing higher charge transfer, the degradation efficiency of the Malachite Green could increase since more hydroxyl (OH) radicals could be generated from the electrons and holes (Marie, et al., 2019). In addition, the high adsorption capacity of carbon also plays an important role in improving the degradation performance of Malachite Green. With the increased surface area, better charge separation, and large adsorption capacity, the degradation efficiency of Malachite Green showed a rapid increase and reached its maximum value in the presence of 10 % C/g-C$_3$N$_4$. This implied that the optimum carbon content in C/g-C$_3$N$_4$ for this study was 10 wt%.

A decrease in degradation efficiency could be observed when the amount of carbon composited on g-C$_3$N$_4$ exceeds 10 wt %. This phenomenon occurred because the concentration of carbon composited with g-C$_3$N$_4$ was extremely high. As the weightage of carbon increased, more black carbon would be composited on the surface of g-C$_3$N$_4$ which blocked the light absorption of g-C$_3$N$_4$ that detriments the sonocatalytic performance (Chen, Kuo and Lu, 2016). Light absorption by g-C$_3$N$_4$ is important since g-C$_3$N$_4$ must be excited by the light generated by acoustic bubbles in order to form electron-hole pairs that generate OH radicals. With some of the light being blocked by carbon, the degradation efficiency of Malachite Green dropped and remained the almost constant for the other three composite samples. Since more carbon would block more light from the absorption of g-C$_3$N$_4$, the degradation efficiency did not show much difference. It was speculated that the high carbon content would have better adsorption of dye as compared to the ones with lower carbon weightage which compromises the decrease in sonocatalytic performance.

For pure carbon, the sonocatalytic performance is very much better than pure g-C$_3$N$_4$. Pure carbon even shows better degradation compared to 5 % C/g-C$_3$N$_4$. The better performance of pure carbon than pure g-C$_3$N$_4$ was accredited to the large surface area of pure carbon. With a larger surface area, the number of acoustic bubbles generated will increase due to heterogeneous nucleation (Khataee, et al., 2014). The

increased number of acoustic bubbles generated would make the sonocatalytic performance better since more OH radicals were generated to degrade the Malachite Green molecules present in the solution.

4.2.2 Effect of Ultrasonic Irradiation on Different Dye

For the effect of different types of dyes, three dyes are selected for this study which are Malachite Green, Methyl Orange, and Acid Orange G with the degradation efficiency of each dye shown in Figure 4.5. The degradation on Malachite Green shows the best results with degradation efficiency at 86.06 %. The degradation performance of Methyl Orange was the lowest (1.54 %) followed by Acid Orange G with a degradation of 9.12 %.
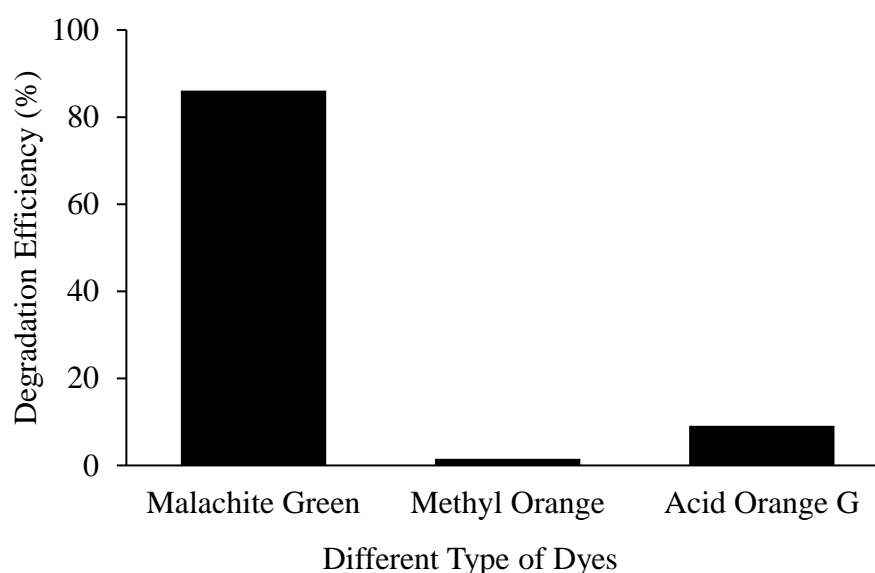
Figure 4.5: Degradation Efficiency of Different Type of Dyes by Using 10 wt% C/g-C_3N_4 (Initial Dye Concentration = 15 ppm, Initial Catalyst Loading = 0.3 g/L, and natural solution pH for 10 Minutes)

Based on Table 3.2, the major category of Methyl Orange and Malachite Green were anionic and cationic dye, respectively. According to Liu, et al. (2016), the degradation performance was affected by the adsorption capability of dye on the catalyst surface. The surface charge of catalysts played an important role in the degradation performance of different dyes (Laid, et al., 2015). The surface charge of g-C_3N_4 was inferred to be negatively charged in aqueous suspension above a solution pH of 4.4 (Zhu, et al., 2015). Since Malachite Green was the only cationic dye among

the three, the adsorption capability of Malachite Green to g-C$_3$N$_4$ would be the best since they possess opposite charges. Anionic dyes possess the same charge as the catalyst surface and tend to repel each other which inhibited the degradation performance. If the target pollutant was far from the catalyst, degradation would not occur since the OH radicals had relatively short lifetimes which means the OH radicals were unlikely to be able to diffuse far from the catalyst surface (Shimizu, et al., 2007). According to Zhou, et al. (2017), the degradation of Methyl Orange by g-C$_3$N$_4$ showed terrible results which coincided with this study due to the similar charges between the surface and the dye molecule.

The degradation efficiency for Acid Orange G is greater than Methyl Orange. This could be explained by comparing their molecular weight. The larger molecular structure of Acid Orange G allowed easier degradation of dye molecule (Abdullah and Pang, 2010). Since Malachite Green showed the highest degradation efficiency among the three dyes studied, Malachite Green will be selected as the targeted dye for the subsequent study.

4.2.3   Effect of Hydrogen Peroxide (H$_2$O$_2$) Dosage

The effect of H$_2$O$_2$ dosage (0 to 1.50 mmol/L) on the degradation efficiency was studied and the results are shown in Figure 4.6. It was noted that the degradation efficiency of Malachite Green was the lowest with a degradation of 91.03 % when there was no H$_2$O$_2$ added. After the addition of H$_2$O$_2$, the degradation of Malachite Green went up to 100 % for every dosage until 0.5 mmol/L. The degradation efficiency of the Malachite Green was dropped from 100 % to 94.89 % when the H$_2$O$_2$ dosage used increased from 0.5 mmol/L to 1.5 mmol/L.

The increment in degradation efficiency after the addition of H$_2$O$_2$ implied that H$_2$O$_2$ will aid in the sonocatalytic degradation process. H$_2$O$_2$ is a strong oxidizing agent that can generate more OH radicals by self-decomposition under ultrasonic irradiation (Farhadi and Siadatnasab, 2016). The increased amount of OH radicals in the solution would improve the degradation performance.

The decrement in the degradation performance was observed when excessive amount of H$_2$O$_2$ was utilised. The decrease in performance could be due to two factors which were the self-quenching process of OH radicals and the scavenging effect for OH radicals. At high concentration of H$_2$O$_2$, hydroperoxyl radicals (OOH•) with lower oxidation potential would be produced instead of OH radicals. The scavenging effect

would reduce the amount of OH radicals and holes present in the solution. A high dosage of H_2O_2 would also increase the toxicity of the solution. Since the degradation efficiency of 10 % $C/g\text{-}C_3N_4$ in the absence of H_2O_2 showed an impressive result of 91.03 %, it was decided that no H_2O_2 would be added for the subsequent studies.
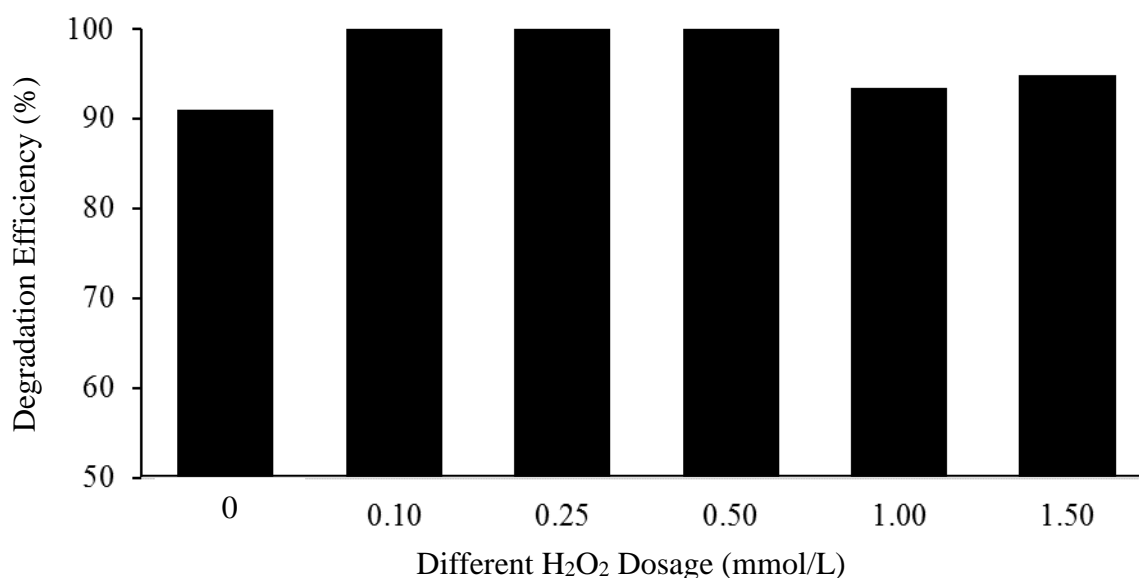
Figure 4.6: Degradation Efficiency of Malachite Green with Different H_2O_2 Dosage by Using 10 wt% $C/g\text{-}C_3N_4$ (Initial Dye Concentration = 15 ppm, Initial Catalyst Loading = 0.3 g/L, and natural solution pH for 10 Minutes)

4.3 Optimisation Studies

For this study, three factors were taken into consideration for the optimisation study which were initial catalyst dosage (g/L), initial dye concentration (ppm), and solution pH. A central composite design was used to analyse the interactive effect for these three parameters on the degradation efficiency of Malachite Green.

4.3.1 Central Composite Design (CCD) Model

The experimental and predicted degradation efficiencies values are presented in Table 4.2. The experimental degradation efficiency of Malachite Green by sonocatalytic degradation in the presence of 10 % $C/g\text{-}C_3N_4$ was found to be in the range of 65.91 % to 97.11 % which was consistent with the predicted degradation efficiencies obtained from the Design Expert 11 (66.75 % to 96.69 %). The residual values between the actual and predicted values are also displayed in Table 4.2. After keying in the

degradation efficiency values based on the experiment, the suggested model to use was quadratic vs 2FI model. This modification was caused by the insignificance of the interaction between initial dye concentration and initial catalyst loading. The p-value for the interaction of these two parameters were 0.1354 which is more than 0.05. Since modelling with insignificant model terms would affect the accuracy of the model, it was decided that the term for interaction between initial dye concentration and initial catalyst loading would be removed to obtain a better model. Hassani, et al. (2015) stated that experimented the initial catalyst dosage between a range of 0.1 g/L and 0.3 g/L reported that the interaction between initial dye concentration and initial catalyst dosage were significant for their model. This implied that the range of values of initial catalyst loading used for modelling should be higher to obtain a significant interaction between initial dye concentration and initial catalyst loading.

The dependent and independent variables could be correlated by using a second-order polynomial response equation (Hassani, et al., 2015). The empirical relationship between the response and independent variables for the sonocatalytic degradation of Malachite Green in the presence of 10 wt% C/g-C_3N_4 were shown in Equation 4.1 and 4.2. The equations provide an approximate function for the response factor. Equation 4.1 shows the second-order polynomial response equation in terms of coded units while Equation 4.2 shows the equation in terms of actual units of the parameters.

$$y_{pred} = 85.69 - 3.09X_1 + 2.92X_2 + 8.31X_3 + 1.66X_1X_3 - 1.79X_2X_3 +$$
$$0.8023X_1X_1 + 1.07X_2X_2 - 1.76X_3X_3 \tag{4.1}$$

where

X_1 = initial dye concentration, ppm

X_2 = initial catalyst loading, g/L

X_3 = pH of solution

y_{pred} = predicted degradation efficiency, %

$$y_{pred} = 166.6090 - 9.0045 * Initial\ Dye\ Concentration - 3.0644 *$$
$$Initial\ Catalyst\ Loading + 5.5349 * pH + 0.3318 *$$
$$Initial\ Dye\ Concentration * pH - 8.9438 * Initial\ Catalyst\ Loading * pH +$$

$$0.1284 * Initial\ Dye\ Concentration^2 + 107.4514 *$$
$$Initial\ Catalyst\ Loading^2 - 0.4389 * pH^2 \tag{4.2}$$

Equation 4.2 provides a much easier calculation since it does not require the conversion of actual values to coded values. The predicted values shown in Table 4.2 were computed by using either Equation 4.1 or Equation 4.2. The small residual values for all the runs indicated that the predicted values were like the experimental values. The sign of the terms in Equation 4.1 and 4.2 implied the effect of that parameter on the degradation efficiency. A positive sign for the term showed synergistic effect on the degradation while a negative sign for the term showed antagonistic effect on the degradation (Pang, Abdullah and Bhatia, 2010). Equations 4.1 and 4.2 could determine the interactive effect between variables and even predict the optimum value of these variables that would provide the best degradation performance.

4.3.2   Regression Analysis of the Model

The suitability of the model is assessed by using the analysis of variance (ANOVA). Table 4.3 presents the summarised results of ANOVA for the central composite design model. The statistical significance of the model could be evaluated by the results of ANOVA. The analysis showed that the coefficient of determination, (R^2) value was very close to unity and had a value of 0.9862 which implied that the predicted value from Equations 4.1 and 4.2 were reliable. The R^2 value of 0.9862 also indicated that 98.62 % of the variations of degradation of Malachite Green could be explained by the model while the remaining 1.38 % of the variations was not taken into account by the model (Hassani, et al., 2015). With the R^2 value close to 1, the model obtained could provide an accurate estimation for the degradation efficiency within the studied range of values.

Table 4.2: The Three Factor Central Composite Design Matrix and Value of Degradation Efficiency

Standard Order	Point Type	Actual and Coded Independent Variable Levels			Degradation Efficiency, %		Residuals
		Initial Dye Concentration, ppm (X_1)	Initial Catalyst Loading, g/L (X_2)	Solution pH (X_3)	Experimental Values	Predicted Values	
1	Factorial	20.00 (-1)	0.300 (-1)	4.0 (-1)	77.62	77.54	0.08
2	Factorial	25.00 (+1)	0.300 (-1)	4.0 (-1)	68.86	68.03	0.83
3	Factorial	20.00 (-1)	0.500 (+1)	4.0 (-1)	88.69	86.96	1.73
4	Factorial	25.00 (+1)	0.500 (+1)	4.0 (-1)	76.12	77.46	-1.34
5	Factorial	20.00 (-1)	0.300 (-1)	8.0 (+1)	94.23	94.42	-0.19
6	Factorial	25.00 (+1)	0.300 (-1)	8.0 (+1)	91.07	91.55	-0.48
7	Factorial	20.00 (-1)	0.500 (+1)	8.0 (+1)	97.11	96.69	0.42
8	Factorial	25.00 (+1)	0.500 (+1)	8.0 (+1)	92.21	93.82	-1.61
9	Axial	18.30 (-1.682)	0.400 (0)	6.0 (0)	91.88	93.16	-1.28
10	Axial	26.70 (+1.682)	0.400 (0)	6.0 (0)	84.23	82.75	1.48
11	Axial	22.50 (0)	0.232 (-1.682)	6.0 (0)	83.60	83.81	-0.21

Standard Order	Point Type	Actual and Coded Independent Variable Levels			Degradation Efficiency, %		Residuals
		Initial Dye Concentration, ppm (X_1)	Initial Catalyst Loading, g/L (X_2)	Solution pH (X_3)	Experimental Values	Predicted Values	
12	Axial	22.50 (0)	0.568 (+1.682)	6.0 (0)	94.05	93.64	0.41
13	Axial	22.50 (0)	0.400 (0)	2.6 (-1.682)	65.91	66.75	-0.84
14	Axial	22.50 (0)	0.400 (0)	9.4 (+1.682)	95.73	94.70	1.03
15	Centre	22.50 (0)	0.400 (0)	6.0 (0)	85.64	85.69	-0.05
16	Centre	22.50 (0)	0.400 (0)	6.0 (0)	84.19	85.69	-1.50
17	Centre	22.50 (0)	0.400 (0)	6.0 (0)	86.85	85.69	1.16
18	Centre	22.50 (0)	0.400 (0)	6.0 (0)	85.23	85.69	-0.46
19	Centre	22.50 (0)	0.400 (0)	6.0 (0)	85.96	85.69	0.27
20	Centre	22.50 (0)	0.400 (0)	6.0 (0)	86.22	85.69	0.53

Table 4.3: ANOVA Results for Sonocatalytic Degradation of Malachite Green

Factors	Sum of Squares	Degree of Freedom	Mean Square	F-value	Probability, P-value	
Modified Model	1316.11	8	164.51	98.10	< 0.0001	Significant
X_1	130.74	1	130.74	77.97	< 0.0001	
X_2	116.72	1	116.72	69.60	< 0.0001	
X_3	942.97	1	942.97	562.31	< 0.0001	
X_1X_3	22.01	1	22.01	13.13	0.0040	
X_2X_3	25.60	1	25.60	15.26	0.0024	
X_1^2	9.28	1	9.28	5.53	0.0384	
X_2^2	16.64	1	16.64	9.92	0.0092	
X_3^2	44.42	1	44.42	26.49	0.0003	
Residual	18.45	11	1.68			
Lack of Fit	14.28	6	2.38	2.86	0.1345	Insignificant
Pure Error	4.16	5	0.83			
Corrected Total	1334.55	19				

$R^2 = 0.9862$; adequate precision = 34.4670

The F-values, P-values, and several other statistical values could be used to determine the significance of the model. All these values could be observed in Table 4.3. The F-value of the model was 98.10 which reflected that the model was significant. The large F-value also implied that there was only a 0.01 % chance that the large value was due to noise. The adequate precision value was a measure of signal to noise ratio. According to Pang, Abdullah and Bhatia (2010), it was best to have the adequate precision value above 4. This model had adequate precision at the value of 34.4670 which implied that the navigation of design space could be done. The large signal to noise ratio indicated that the effect of noise on this model was very small.

The lack of fit test for this model was insignificant. The F-value and P-value for lack of fit were 2.86 and 0.1345, respectively. The lack of fit test was a test that compared the residual error and pure error from the replicated design points. If the lack

of fit test was significant, it would imply that the model analysed was not the most appropriate model. A model with a significant lack of fit should not be used to predict the response factor (Stat-Ease, 2018). With a F-value of 2.86 for the lack of fit test, it implied that the lack of fit was insignificant relative to the pure error. The large F-value for lack of fit test indicated that there was a 13.45 % chance the F-value was caused by noise. A significant lack of fit test would displayed a P-value that was lower or equal to 0.10 (Stat-Ease, 2018).

Next, the significance of each term in the model was analysed. The significance of the modelling terms was based on their respective P-values. The P-value was a probability value that indicated the proportion of F-distribution that goes beyond the observed F-value (Pang, Abdullah and Bhatia, 2010). For terms that had P-values greater than 0.1, the term would be insignificant to the model and the removal of the term was acceptable since it did not affect the model. The interaction coefficient between initial dye concentration and initial catalyst loading was removed from the model since it had P-value of 0.1354 which was greater than 0.1. This indicated that the term would be insignificant to the model and removing it would improve the model. The rest of the quadratic terms had P-values that were less than 0.05. These modelling terms were said to be significant because their P-values were lower than 0.05 and needed to be included in the model. By looking at the P-values, the terms that were significant in determining the predicted degradation efficiency were all the individual variable effect terms, all the quadratic terms and only two of the interaction terms which were X_1, X_2, X_3, X_1^2, X_2^2, X_3^2, X_1X_3, and X_2X_3.

Figure 4.7 shows the actual and predicted degradation values of Malachite Green. The linear line indicated the predicted degradation value while the plots were the actual degradation value obtained from experimental work. The plots were not that far away from the linear line which implied that the actual and predicted degradation values were in good agreement and showed satisfactory correlation between the values. With the predicted and actual degradation values so similar, the model developed was said to be suitable for predicting the degradation efficiency of Malachite Green in the conditions investigated.
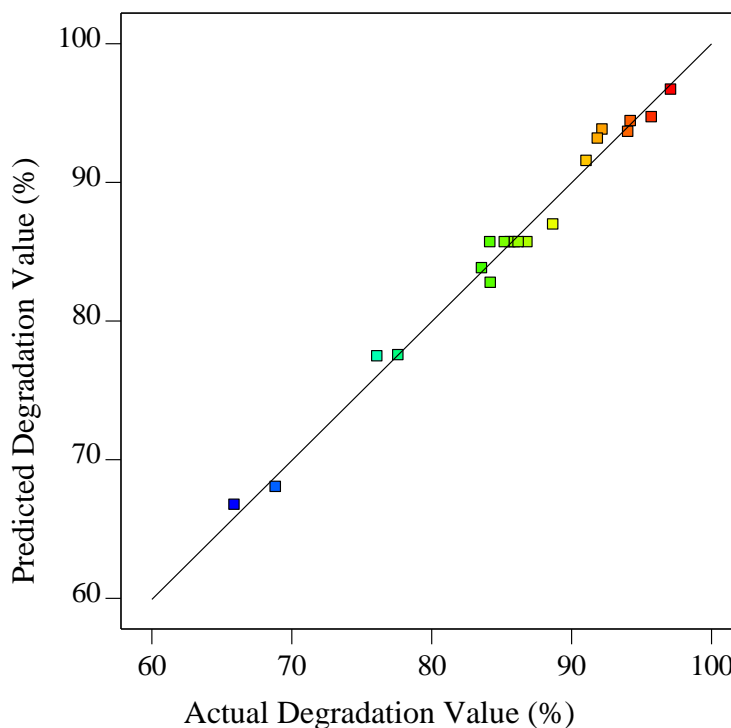
Figure 4.7: Predicted and Actual Values of Sonocatalytic Degradation of Malachite Green ($R^2 = 0.9862$)

4.3.3   The Effect of Operational Parameters

Design Expert 11 was used to study three factors which were the initial dye concentration, initial catalyst loading, and solution pH. The interaction between these factors and their effect on the degradation efficiency was investigated. The study of interaction between initial dye concentration and initial catalyst loading was excluded because the ANOVA results showed that the interaction was insignificant to the degradation efficiency of Malachite Green. The interactive effect of the selected factors could be understood better by using three-dimensional response surface plots and two-dimensional contour plots (Hassani, et al., 2015). Before analysing the interactive effect of these three factors, the effect of the three factors individually were assessed by using a perturbation plot.

The perturbation plot for this model is shown in Figure 4.8. The perturbation plot could allow a quick identification of the effective parameters on the response factor (Hassani, Eghbali and Metin, 2018). The most effective factor on the degradation efficiency should have the steepest curve in the perturbation plot. The three factors shown in Figure 4.8 were initial dye concentration (A), initial catalyst

loading (B), and solution pH (C). The factor of solution pH showed the steepest curve in the plot. This implied that solution pH was the most effective parameter in affecting the degradation efficiency of Malachite Green among the three factors being studied. This result was in accordance with the results obtained by ANOVA that showed the solution pH parameter had the largest F-value. The relatively flat curve for the initial catalyst loading parameter implied that the increased in catalyst loading had negligible effect on the degradation efficiency compared to the other factors. The positive gradient shown in the curves for initial catalyst loading and solution pH indicated that the increase in value for these parameters would result in an increase in degradation efficiency of Malachite Green. On the other hand, a negative gradient like the one for initial dye concentration would indicate that an increase in this factor would reduce the degradation efficiency.
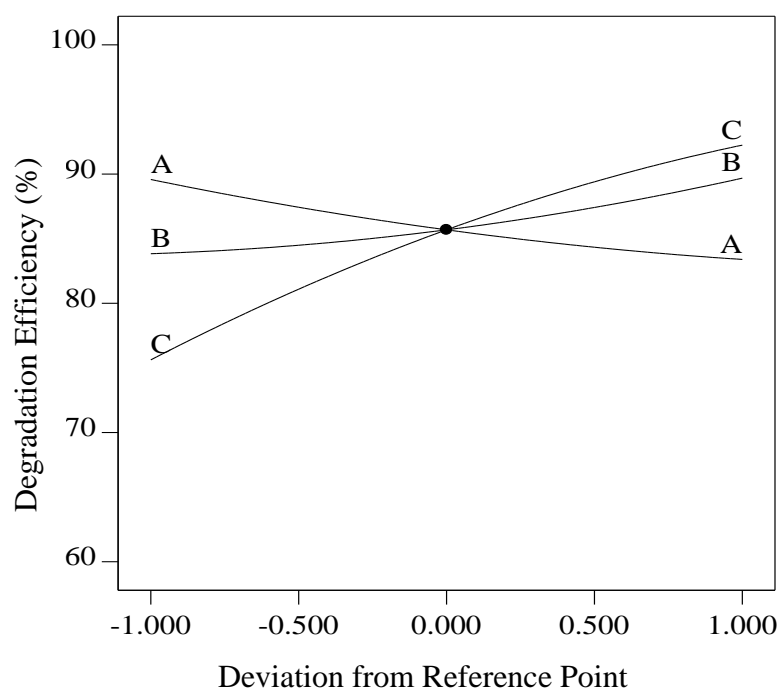
Figure 4.8: Perturbation Plot for the Three Factors Studied

Figure 4.9 shows the three-dimensional response surface plot of degradation efficiency with solution pH and initial dye concentration. The three-dimensional surface indicated that an increase or decrease in solution pH would greatly affect the degradation efficiency as shown from the perturbation plot. Run 13 and 14 which had a degradation efficiency of 66.75 % and 94.70 %, respectively indicated that solution

pH greatly affected the degradation efficiency of Malachite Green. For the effect of initial dye concentration, run 9 and 10 that had the degradation efficiency of 93.16 % and 82.75 %, respectively showed that the change in initial dye concentration did not affect the response factor greatly. By comparing run 1 and run 6, the interaction between the two factors being studied could be observed. Run 1 was being conducted at a lower solution pH and initial dye concentration demonstrated a degradation efficiency of 77.62 %. Meanwhile, run 6 that was performed at a higher solution pH and initial dye concentration showed a higher degradation efficiency of 91.07 %. This comparison showed that solution pH was the major factor that affected the response factor while the initial dye concentration only affected the degradation efficiency by a small fraction as compared to solution pH.
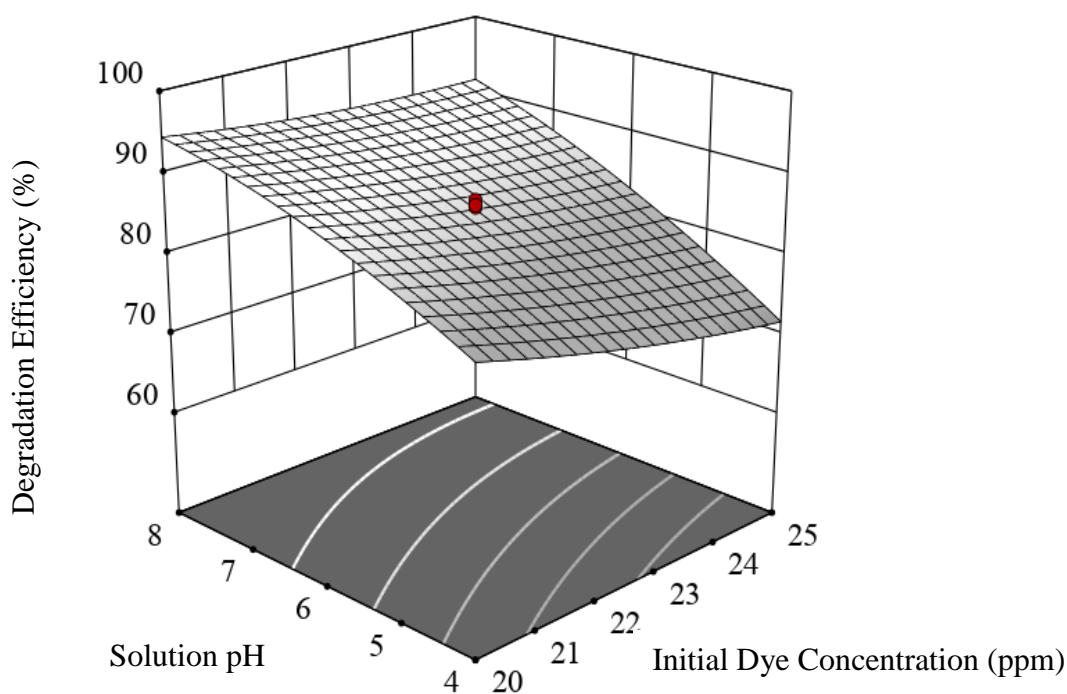

Figure 4.9: Three-dimensional Response Surface Plot of Degradation Efficiency of Malachite Green Against Solution pH and Initial Dye Concentration (Initial Catalyst Loading = 0.4 g/L for 10 Minutes)

Thus, the parameter that affected the degradation efficiency the most was the solution pH. A change in solution pH could affect the electrostatic interaction between

the dye molecule and catalyst surface. Solution pH variation could also alter the production of radicals that directly affected the degradation efficiency. When solution pH was increased towards the alkaline region, the degradation efficiency of Malachite Green was increased greatly. This phenomenon could be explained by the increased production of OH radicals (Lekshmi, Yesodharan and Yesodharan, 2018). The alkaline conditions implied that more hydroxyl ions would be present in both the catalyst surface and cavitation bubbles (Bampos and Frontistis, 2019). With more hydroxyl ions being converted to OH radicals, the degradation of Malachite Green could be improved greatly. When the solution went toward the acidic region, the degradation efficiency of Malachite Green dropped drastically. This anomaly was caused by the presence of excess hydrogen ions in the dye solution. The hydrogen ions would compete with Malachite Green molecules to adsorb on the catalyst surface (Soni, Tiwari and Bajpai, 2013). This greatly decreased the degradation efficiency since the dye molecules could only be degraded by OH radicals formed from acoustic cavitation. According to Bampos and Frontistis (2019), chloride ions that was used to adjust the solution pH would scavenge OH radicals and caused the radicals to convert back to hydroxyl ions. The scavenging effect was displayed in Equation 4.3.

$$2 \bullet OH + Cl^- \rightarrow OH^- + \bullet ClOH^- \tag{4.3}$$

The scavenging effect of chloride ions and adsorption of hydrogen ions on the catalyst surface explained the reduction of degradation efficiency of Malachite Green at acidic conditions.

The initial dye concentration was another factor that would affect the degradation efficiency of Malachite Green. The increase in initial dye concentration would cause a slight decrease in the response factor. This trend could be explained by both physical and chemical processes. The mass transfer limitations between the dye molecules and catalyst surface was the physical process while the concentration of radical species, mostly OH radicals, was the chemical process. At higher initial dye concentration, the amount of dye molecules present in the solution would increase which caused the adsorption sites of the catalyst surface or cavity surface to be limited. The chemical process was limited by the concentration of radical species in the solution. With the increase in initial dye concentration, the amount of generated OH

radicals remained the same. This caused the amount of OH radicals to become the rate limiting step that reduce the degradation efficiency (Bampos and Frontistis, 2019). The increase in initial dye concentration would decrease the degradation efficiency of Malachite Green might due to the limiting factors which were the concentration of radical species present and the availability of adsorption sites on the catalyst surface.

The interaction between solution pH and initial catalyst loading is shown in Figure 4.10. The curve shown in Figure 4.10 indicated that solution pH affected the degradation efficiency more than the initial catalyst loading. This relation was shown in their difference in F-values from the ANOVA results. The initial catalyst dosage had the lowest F-value among three factors which implied that it might affect the degradation efficiency insignificantly. By comparing run 11 and run 12, the degradation efficiency shown by these runs were 83.60 % and 94.05 %, respectively. The difference between run 11 and run 12 was only the initial catalyst dosage used. Based on the curvature in Figure 4.10, the initial catalyst dosage showed the least effect on the response factor when the solution pH was at alkaline condition. The interaction could be done by comparing four runs which were run 1, run 3, run 5, and run 7. Run 1 and run 3 showed a degradation efficiency of 77.62 % and 88.69 % at low solution pH when the initial catalyst loading was varied. Run 5 and run 7 showed the degradation efficiency of Malachite Green of 94.23 % and 97.11 % at solution pH 8 when initial catalyst loading was increased.

The third factor that was studied in this model was the initial catalyst dosage. An increase in initial catalyst dosage would cause a slight increase in the response factor. This phenomenon could be explained by the increase in surface area of the catalyst (Hassani, Eghbali and Metin, 2018). The increased surface area for the catalyst provided more active sites for the nucleation of bubbles and the generation of free radicals (Pang, Abdullah and Bhatia, 2010). When more radicals were produced, the degradation performance would be improved due to the generation of free radicals to oxidise the Malachite Green molecules. The insignificant effect of initial catalyst loading at high solution pH might be due to the presence of hydroxyl ions in the solution. With more hydroxyl ions, the amount of OH radicals produced could be greatly increased which caused the increase in catalyst to be redundant. The increase in initial catalyst loading would improve the degradation performance by generating

more radicals but the effect would be insignificant once exceed the optimum amount of radicals in the solution.
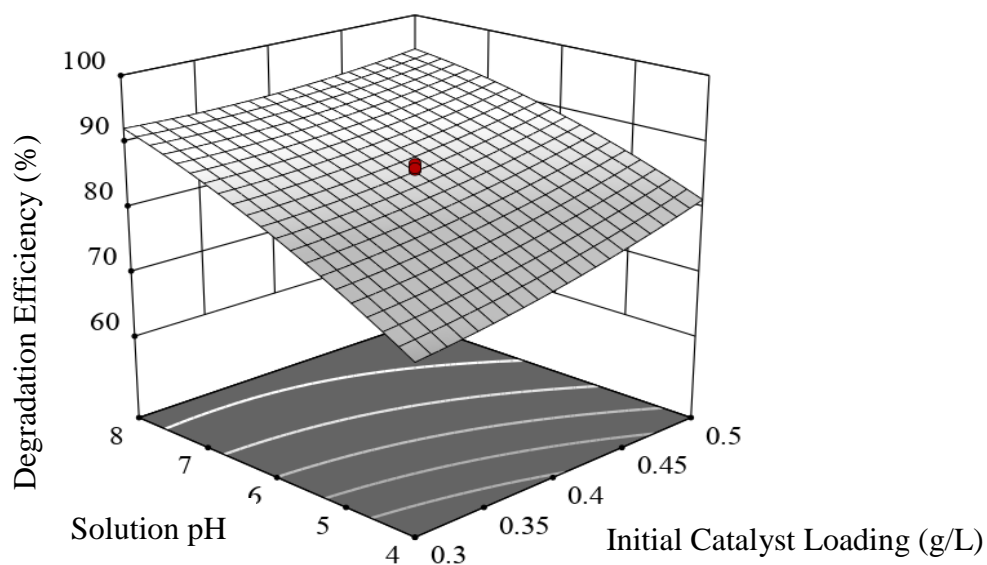
Figure 4.10: Three-dimensional Response Surface Plot of Degradation Efficiency of Malachite Green Against Solution pH and Initial Catalyst Dosage (Initial Dye Concentration = 22.5 ppm for 10 Minutes)

4.3.4 Optimisation and Model Validation

The optimisation and model validation run are conducted simultaneously, and the results is shown in Table 4.4. The response surface methodology (RSM) was used to obtain the optimum values of the three independent variables used for the CCD model. Three independent variables were initial dye concentration, initial catalyst loading, and solution pH. The solution selected from the numerical optimisation showed the highest desirability which was 0.986. The values of the optimum operational parameters for initial dye concentration, initial catalyst loading, and solution pH were 20 ppm, 0.5 g/L, and 8, respectively. The predicted and experimental values for degradation efficiency of Malachite Green were 96.69 % and 97.11 %, respectively. The percentage error for the predicted and actual value was only 0.43 %. The low percentage error between the two values indicated that the applied model was reliable to make predictions on the response factor for real conditions.

Table 4.4: Model Validation Conducted at Optimum Condition as Obtained from RSM

Variable	Value
Initial Dye Concentration (ppm)	20
Initial Catalyst Loading (g/L)	0.5
Solution pH	8
Predicted Degradation Efficiency (%)	96.69
Actual Degradation Efficiency (%)	97.11
Percentage Error (%)	0.43

The chemical oxygen demand (COD) for the optimum operational parameters was also analysed. With a degradation efficiency of 97.11 %, the COD removal obtained was only 38.52 % with the initial COD at 135 mg/L and the final COD at 83 mg/L. The low COD removal of the solution indicated that the degradation of the Malachite Green molecule was not complete. Theoretically, the degraded dye molecule should convert to CO_2 and H_2O as its final product. Instead, it was speculated that the dye molecules were only degraded to the point where it lost its colour. Since the colour of a dye was based on the conjugated system of the structure and not the whole molecule, the decolourisation of solution did not imply that all the dye molecules in the solution were being converted to CO_2 and H_2O. The degradation efficiency value was obtained based on the absorbance of visible light at a wavelength of 617 nm. Since OH radicals only tackle the conjugated system of the dye molecules to decolourise the solution, the remaining molecules might still be remained in the solution. According to Pang, Abdullah and Bhatia (2010), the low COD removal was caused by the presence of reducible species such as H_2O_2 that was produced during the ultrasonication of water. The degradation efficiency of Malachite Green did not directly relate to the COD removal of the solution since there might be some colourless compound in the treated solution.

4.4　Reusability of 10 % C/g-C₃N₄ catalyst

The reusability of a catalyst was an important factor to determine the practicality of using the studied catalyst for wastewater treatment processes. Although the cost of producing 10 wt% C/g-C₃N₄ was low since it was derived from biomass and urea, the reusability of the catalyst was still an important factor to reduce waste production.

Figure 4.11 shows the degradation efficiency of Malachite Green for the fresh catalyst and the two consecutive runs to test the reusability of the said catalyst. The degradation efficiency for the first, second, and third run were 95.32 %, 93.24 %, and 88.04 %, respectively. The decrement in degradation efficiency for the reused runs could be explained by two factors. The first factor was the loss of catalyst during the centrifugation and rinsing process. The loss of catalyst was caused by the hydrophilicity of the 10 wt% C/g-C₃N₄. The presence of functional groups such as carbonyl (C=O), hydroxyl (-OH) on the catalyst surface caused the catalyst to be hydrophilic. The reused sample would have lower initial catalyst loading for each repeated run since it could bind with water molecules easily to form hydrogen bonds (Thue, et al., 2017). The second factor was the partial disintegration caused by ultrasonic irradiation. The movement of liquid under ultrasonic irradiation created a strong mechanical force that would partially disintegrate the catalyst surface. The disintegration effect would disrupt the active sites of the catalyst and inhibited the generation of OH radicals (Abdullah and Pang, 2010).
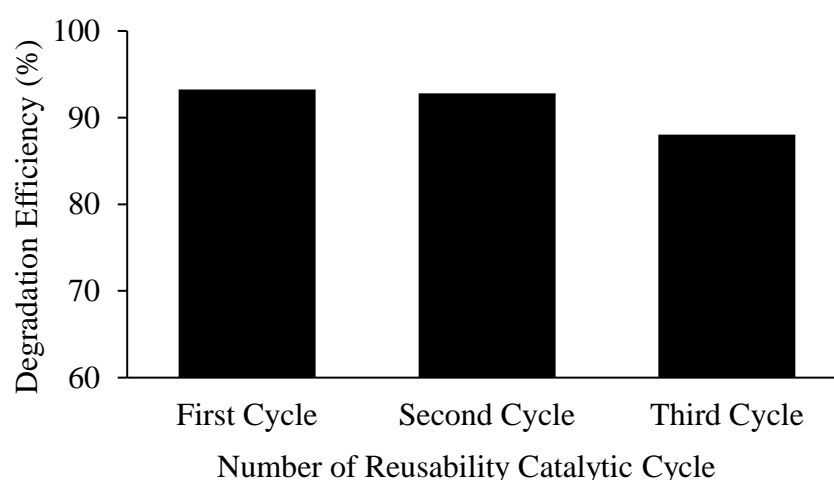
Figure 4.11: Degradation Efficiency of Malachite Green with Three Reusability Catalytic Cycle (Initial Dye Concentration = 15 ppm, Initial Catalyst Loading = 1 g/L, and natural solution pH for 10 Minutes)

4.5   Possible Mechanisms for Degradation of Malachite Green

Figure 4.12 shows the degradation efficiency for adsorption and sonocatalytic degradation. With the incorporation of carbon in the 10 wt% C/g-C_3N_4, one might infer that the degradation of Malachite Green could be due to the adsorption of carbon rather than sonocatalytic degradation. The degradation efficiencies obtained were 93.44 % and 7.68 % for sonocatalytic degradation and adsorption, respectively. The results proved that the sonocatalytic degradation of Malachite Green using 10 wt% C/g-C_3N_4 was contributed by the ultrasonication rather than adsorption.
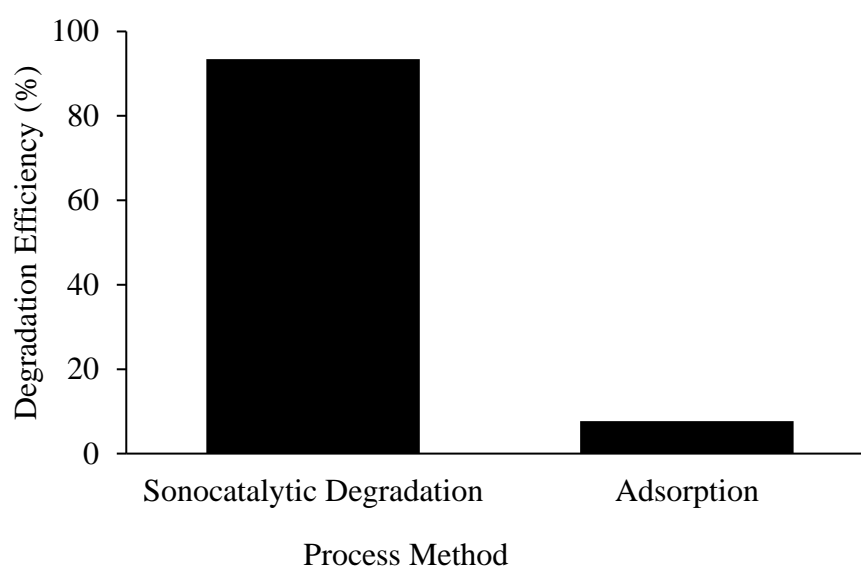
Figure 4.12: Degradation Efficiency when Different Type of Degradation Method is Used (Initial Dye Concentration = 15 ppm, Initial Catalyst Loading = 0.3 g/L, and natural solution pH for 10 Minutes)

After confirming that the degradation method used was sonocatalysis, the possible mechanism for the degradation of Malachite Green could be discussed. There were two possible mechanisms that degraded the Malachite Green molecule. The first mechanism required the presence of 10 wt% C/g-C_3N_4. The sonocatalyst would absorb the light released during sonoluminescence (SL) to excite its electrons. Once light was absorbed, the electrons in the valence band (VB) of the sonocatalyst would be excited to the conduction band (CB) which would leave a hole at the VB (Zaman, et al., 2017). This would cause the formation of the electron-hole pair. The electron in the CB had strong reduction potential that would reduce the oxygen present in the solution to a

free radical that was known as superoxide ions ($O_2^-\bullet$). The holes left in the VB would have high oxidising potential that would be able to oxidise the water molecules and produce OH radicals. The free radicals generated would degrade the dye molecule. The second mechanism was the ultrasonic irradiation in water medium which would generate OH and H radicals that could also degrade the dye molecules in the solution (Karaca, et al., 2016). Both mechanisms led to the generation of radicals which implied that the Malachite Green molecule was degraded by the free radicals in the solution.

4.6   Summary of Chapter 4

This chapter includes the results and discussion obtained from the experimental work. The characterisation of pure g-C_3N_4, pure carbon, and carbon/g-C_3N_4 composite at different weight percentages by XRD, SEM-EDX, and FTIR were included in this chapter. The optimum condition of the various parameters analysed was also found out. The incorporation of 10 wt% of carbon with g-C_3N_4 shows the best degradation efficiency. Malachite Green showed the best degradation efficiency among Methyl Orange, Acid Orange G, and Malachite Green. It was decided that no H_2O_2 should be used for subsequent studies because the degradation efficiency without it is acceptable and it is a toxic chemical. The optimum condition after investigating the interactions between initial dye concentration, initial catalyst loading, and solution pH were 20 ppm, 0.5 g/L, and 8.

CHAPTER 5

CONCLUSIONS AND RECOMMENDATIONS

5.1   Conclusions

Pure graphitic carbon nitride (g-C_3N_4) and carbon/g-C_3N_4 composite at different weight percentages was prepared by pyrolysis at 500 ^{O}C for 2 hours. The characteristics for pure g-C_3N_4, pure carbon, and carbon/g-C_3N_4 composite at different weight percentages were studied by using X-ray diffraction (XRD), scanning electron microscopy-energy dispersive X-ray (SEM-EDX), and fourier-transform infrared (FTIR) analysis. The XRD patterns indicated that pure g-C_3N_4 exhibited characteristic peaks at 27.5^o, and 44.1^o. The incorporation of carbon with g-C_3N_4 resulted in a loss of the characteristic peaks of pure g-C_3N_4. As the weightage of carbon increased, the XRD pattern of the composite samples showed no sign of the characteristic peaks of g-C_3N_4 but only a broad peak that was similar with pure carbon could be observed. The SEM images showed that pure g-C_3N_4 had a structure that resembles overlapping flat sheets with irregular shape and irregular porous. When carbon was composited with g-C_3N_4, a smooth surface with the irregular-shaped particles could be observed. With the increasing weightage of carbon amount, the irregular-shaped particles were decreased. The presence of irregular-shaped particles was not observed in the SEM image of pure carbon. The EDX results showed that the pure g-C_3N_4 had a carbon to nitrogen ratio of 0.78 which was close to the stoichiometric carbon to nitrogen ratio of 0.75. The addition of carbon in composite samples increased the weight percentage of carbon up to 90 wt%. The FTIR results obtained was consistent with the XRD patterns. The peaks of pure g-C_3N_4 was disappeared when increasing the amount of carbon in the composite samples. The FTIR results for 15 wt% C/g-C_3N_4, 20 wt% C/g-C_3N_4, and 25 wt% C/g-C_3N_4 were observed to be similar with the FTIR result of pure carbon.

The effect of various parameters was also studied to determine the optimum conditions for sonocatalytic degradation of organic dyes. The parameters studied were carbon amount composited with g-C_3N_4, various types of organic dyes, and hydrogen peroxide (H_2O_2) dosage. 10 wt% C/g-C_3N_4 showed the best degradation efficiency of Malachite Green with a value of 93.44 %. The degradation of organic dyes (Malachite Green, Methyl Orange, Acid Orange G) relied on the surface charge of the catalyst and

the dye molecules themselves. Malachite Green showed the best degradation efficiency in the presence of 10 wt% C/g-C_3N_4 because Malachite Green was the only cationic dye being studied, while the surface charge of the catalyst was negative at the natural solution pH. The addition of H_2O_2 during the sonocatalytic degradation of Malachite Green could accelerate the degradation efficiency up to 100 %. Although the incorporation of H_2O_2 increased the degradation efficiency of Malachite Green, it was decided that no H_2O_2 should be used due to the toxicity of the chemical.

The optimisation study was conducted by using Design Expert 11 with a Central Composite Design (CCD) model. Three factors which were initial dye concentration, initial catalyst loading, and solution pH were studied for this model. The empirical relationship between these three factors had been developed. The interactions between the factors were also analysed and explained. The model was validated by comparing the actual degradation efficiency (97.11 %) of Malachite Green with the predicted value (96.69 %) from the model. It was found that the percentage error between both values were only 0.43 %. The reusability study of 10 wt% C/g-C_3N_4 was also studied. The reused sample showed high sonocatalytic degradation performance even after three catalytic cycles.

5.2 Recommendations for Future Work

The surface area of pure g-C_3N_4, pure carbon, and carbon/g-C_3N_4 composite at different weight percentages should be studied by using Brunauer-Emmett-Teller (BET) surface analysis. According to Marie, et al. (2019), the incorporation of carbon with g-C_3N_4 would increase the surface area of the samples. This characterisation would be useful since sonocatalytic activity of the samples were greatly based on the specific surface area of the samples. With a larger surface area, the generation of OH radicals will be increased which in turn increases the degradation performance of the sample. Therefore, the characterisation of BET to study the surface area of the samples are important for better insight.

After conducting the optimisation study, the interaction between initial dye concentration and initial catalyst loading was omitted from the model due to the insignificance of the interaction. This might be due to by the small range of initial catalyst loading used for the model study. In order to have a better understanding on

the effect of the initial catalyst loading, larger range of values should be used for future study.

REFERENCES

Abbasi, M. and Asl, N. R., 2008. Sonochemical degradation of basic blue 41 dye assisted by nano-TiO$_2$ and H$_2$O$_2$. 153, pp. 942–947.

Abdullah, A. Z. and Pang, Y. L., 2010. Heat treatment effects on the characteristics and sonocatalytic performance of TiO$_2$ in the degradation of organic dyes in aqueous solution. *Journal of Hazardous Materials*, 173(1–3), pp. 159–167.

Afroz, R. and Rahman, A., 2017. Health impact of river water pollution in Malaysia. *International Journal of Advanced and Applied Science*, 4(5), pp. 78–85.

Agarwal, V., Kaur, R. and De, D., 2017. Scenario analysis of textile industry in asia-pacific trade agreement (APTA). *Procedia Computer Science*, 122, pp. 685–690.

An, X., Cao, Y., Liu, Q., Chen, L., Lin, Z., Zhou, Y. and Zhang, Z., 2017. Graphitic carbon/carbon nitride hybrid as metal-free photocatalyst for enhancing hydrogen evolution. *Applied Catalysis A*, 546(7), pp. 30–35.

Ashfaq, a. and Khatoon, a., 2014. Waste management of textiles : A solution to the environmental pollution. *International Journal of Current Microbiology and Applied Sciences*, 3(7), pp. 780–787.

Bampos, G. and Frontistis, Z., 2019. Sonocatalytic degradation of butylparaben in aqueous phase over Pd/C nanoparticles. *Environmental Science and Pollution Research*, pp. 1-15.

Bang, J. H. and Suslick, K. S., 2010. Applications of ultrasound to the synthesis of nanostructured materials. *Advanced Materials*, pp. 1039–1059.

Benkhaya, S., Harfi, S.El. and Harfi, A.El., 2017. Classifications, properties and applications of textile dyes : A review. *Applied Journal of Environmental Engineering Science*, 3(1), pp. 311–320.

Berthomieu, C. and Hienerwadel, R., 2009. Fourier transform infrared spectroscopy. *Photosynthesis Research*, 101(2–3), pp. 157–170.

Bunaciu, A. A., Aboul-Enein, H. Y. and Fleschin, S., 2010. Application of fourier transform infrared spectrophotometry in pharmaceutical drugs analysis. *Applied Spectroscopy Reviews*, 45(3), pp. 206–219.

Bunaciu, A. A., Udriştioiu, E. G. and Aboul-Enein, H. Y., 2015. X-Ray diffraction: Instrumentation and applications. *Critical Reviews in Analytical Chemistry*, 45(4), pp. 289–299.

Cetinkaya, S. G., Morcali, M. H., Akarsu, S., Ziba, C. A. and Dolaz, M., 2018. Comparison of classic fenton with ultrasound fenton processes on industrial textile wastewater. *Sustainable Environment Research*, 28(4), pp. 165–170.

Chandran, D., 2015. A review of the textile industries waste water treatment methodologies. *International Journal of Scientific & Engineering Research*, 7(1), pp. 392–403.

Chen, X., Kuo, D. H. and Lu, D. F., 2016. Nanonization of g-C_3N_4 with the assistance of activated carbon for improved visible light photocatalysis. *RSC Advances*, 6(71), pp. 1-31.

Choudhary, O. P. and Priyanka., 2017. Scanning electron microscope: Advantages and disadvantages in imaging components. *International Journal of Current Microbiology and Applied Sciences*, 6(5), pp. 1877–1882.

Chu, S., Wang, Y., Guo, Y., Feng, J., Wang, C., Luo, W., Fan, X. and Zou, Z., 2013. Band structure engineering of carbon nitride : In search of a polymer photocatalyst with high photo-oxidation property. *American Chemical society: Catalysis*, 3(5), pp. 912-919.

Dehghan, S., Kakavandi, B. and Kalantary, R. R., 2018. Heterogeneous sonocatalytic degradation of amoxicillin using ZnO/Fe_3O_4 magnetic nanocomposite: Influential factors, reusability and mechanisms. *Journal of Molecular Liquids*, 264, pp. 98–109.

Department of Environment, 2010. *Environmental requirements: A guide for investors.*

Department of Environmental, 2016. *Malaysia environmental quality report 2016.*

Department of Statistics, Malaysia, 2016. *Economic census: Environmental compliance 2016*. Jabatan Perangkaan Malaysia.

Dong, G., Zhang, Y., Pan, Q. and Qiu, J., 2014. A fantastic graphitic carbon nitride material : Electronic structure , photocatalytic and photoelectronic properties. *Journal of Photochemistry & Photobiology*, 20, pp. 33–50.

Fang, J., Fan, H., Li, M. and Long, C., 2015. Nitrogen self-doped graphitic carbon nitride as efficient visible light photocatalyst for hydrogen evolution. *Journal of Materials Chemistry A*, 3(26), pp. 13819–13826.

Farhadi, S. and Siadatnasab, F., 2016. Co-Fe_2O_4-CdS nanocomposite : Preparation , characterisation , and application in sonocatalytic degradation of organic dye pollutants, 37(9), pp. 1487–1495.

Flannigan, D. J. and Suslick, K. S., 2005. Plasma formation and temperature measurement during single-bubble cavitation. *Nature*, 434(7029), pp. 52–55.

Goh, P. S. and Ismail, A. F., 2018. A review on inorganic membranes for desalination and wastewater treatment. *Desalination*, 434, pp. 60–80.

Gonawala, K. H. and Mehta, M. J., 2014. Removal of color from different dye wastewater by using ferric oxide as an adsorbent. *International Journal of Engineering Research and Applications*, 4(5), pp. 102–109.

Gong, C. and Hart, D. P., 1998. Ultrasound induced cavitation and sonochemical yields. *The Journal of the Acoustical Society of America*, 104(5), pp. 2675–2682.

Guo, Y., Mi, X., Li, G. and Chen, X., 2017. Sonocatalytic degradation of antibiotics tetracycline by Mn-modified diatomite, 2017. *Journal of Chemistry*, pp. 1-8.

Gürses, A., Açıkyıldız, M., Güneş, K. and Gürses, M. S., 2016. Dyes and pigments. *SpringerBriefs in Green Chemistry for Sustainability*, 8(83), pp. 13-27.

Hassani, A., Darvishi, R., Soltani, C., Kıranşan, M., Karaca, S., Karaca, C. and Khataee, A., 2015. Ultrasound-assisted adsorption of textile dyes using modified nanoclay: Central composite design optimization. *Journal Of Chemical Engineering*, 33(1), pp. 178–188.

Hassani, A., Eghbali, P. and Metin, Ö., 2018. Sonocatalytic removal of methylene blue from water solution by cobalt nanocomposites: response surface methodology approach. *Environmental Science And Pollution Research*, 25(32), pp. 1-16.

Heymann, L., Schiller, B., Noei, H., Stierle, A. and Klinke, C., 2018. A new synthesis approach for carbon nitrides : Polytriazine imide and its photocatalytic properties. *Americal Chemical Society Omega*, 3(4), pp. 3892-3900.

Hong, Y., Meng, Y., Zhang, G., Yin, B., Zhao, Y., Shi, W. and Li, C., 2016. Facile fabrication of stable metal-free $CQDs/g-C_3N_4$ heterojunctions with efficiently enhanced visible-light photocatalytic activity. *Separation and Purification Technology*, 171, pp. 229–237.

Hossain, L., Sarker, S. K. and Khan, M. S., 2018. Evaluation of present and future wastewater impacts of textile dyeing industries in Bangladesh. *Environmental Development*, 26, pp. 23–33.

Hunger, K., 2002. *Industrial Dyes: Chemistry, Properties, Applications.* Frankfurt, Germany: WILEY-VCH.

Joshi, M., Bansal, R. and Purwar, R., 2003. Colour removal from textile effluents. *Indian Journal od Fibre & Textile Research*, 29, pp. 239–259.

Karaca, M., Kiranşan, M., Karaca, S., Khataee, A. and Karimi, A., 2016. Sonocatalytic removal of naproxen by synthesized zinc oxide nanoparticles on montmorillonite. *Ultrasonics Sonochemistry*, 31, pp. 250–256.

Kaur, P., Kushwaha, J. P. and Sangal, V. K., 2018. Transformation products and degradation pathway of textile industry wastewater pollutants in electro-fenton process. *Chemosphere*, 207, pp. 690–698.

Khataee, A., Saadi, S., Vahid, B. and Joo, S. W., 2016. Sonochemical synthesis of holmium doped zinc oxide nanoparticles: Characterization, sonocatalysis of reactive orange 29 and kinetic study. *Journal of Industrial and Engineering Chemistry*, 35, pp. 167–176.

Khataee, A., Sheydaei, M., Hassani, A., Taseidifar, M. and Karaca, S., 2014. Sonocatalytic removal of an organic dye using TiO_2/ Montmorillonite nanocomposite. *Ultrasonics Sonochemistry*, 39, pp. 120–128.

Khataee, A., Soltani, R. D. C., Karimi, A. and Joo, S. W., 2015. Sonocatalytic degradation of a textile dye over Gd-doped ZnO nanoparticles synthesized through sonochemical process. *Ultrasonics Sonochemistry*, 23, pp. 219–230.

Kumar, A. and Konar, A., 2011. Dyeing of Textiles with Natural Dyes. *Natural Dyes*, pp. 29-52.

Laid, N., Bouanimba, N., Zouaghi, R. and Sehili, T., 2015. Comparative study on photocatalytic decolorization of an anionic and a cationic dye using different TiO_2 photocatalysts. *Desalination and Water Treatment*, 47(41), pp. 19357-19373.

Lekshmi, K. P. V., Yesodharan, S. and Yesodharan, E. P., 2018. MnO_2 efficiently removes indigo carmine dyes from polluted water. *Heliyon*, 4(11).

Li, H., Ha, C., and Kim, I., 2009. Fabrication of carbon nanotube/SiO_2 and carbon nanotube/SiO_2/Ag nanoparticles hybrids by using plasma treatment. *Nanoscale Research Letters*, 4(11), pp. 1384–1388.

Li, S., Wang, G., Qiao, J., Zhou, Y., Ma, X., Zhang, H., Li, G., Wang, J. and Song, Y., 2018. Sonocatalytic degradation of norfloxacin in aqueous solution caused by a novel Z-scheme sonocatalyst, mMBIP-MWCNT-In_2O_3 composite. *Journal of Molecular Liquids*, 254, pp. 166–176.

Liu, J., Zhang, T., Wang, Z., Dawson, G. and Chen, W., 2011. Simple pyrolysis of urea into graphitic carbon nitride with recyclable adsorption and photocatalytic activity. *Journal Of Materials Chemistry*, 21(38), pp. 14398–14401.

Liu, Q., Wang, X., Li, Y., Kong, F. and Wang, S., 2016. Visible light catalytic degradation of dye wastewater using carbon nitride. *Environmental and Chemical Science*, pp. 208–213.

Liu, X., Tang, T., Yu, W. and Pipes, R. B., 2018. Multiscale modeling of viscoelastic behaviors of textile composites. *International Journal of Engineering Science*, 130, pp. 175–186.

López-pe, J. J., Velo-Gala, I., Sanchez-Polo, M. and Rivera-Utrilla, J., 2013. Activated carbon as photocatalyst of reactions in aqueous phase. *Applied Catalysis B : Environmental*, 143, pp. 694–704.

Lorimer, J. P., Mason, T. J., Plattes, M., Phull, S. S. and Walton, D. J., 2001. Degradation of dye effluent. *Pure and Applied Chemistry*, 73(12), pp. 1957–1968.

Lyon, F., 2010. General introduction to the chemistry of dyes. *IARC Monographs on the Evaluation of Carcinogenic Risks to Humans*, pp. 55–67.

Makama, A. B., Umar, M. and Saidu, S. A., 2018. CQD-based composites as visible-light active photocatalysts for purification of water. *Visible-Light Photocatalysis of Carbon-Based Materials*, 7, pp. 111-127.

Makowski, S. J., 2012. *Molecular s-triazine and s-heptazine derivatives as building blocks in coordination networks, molecular salts and supramolecular materials*. Ludwig Maximilian University of Munich.

Marcì, G. and Palmisano, L., 2018. Polymeric carbon nitride as heterogeneous photocatalyst for selective oxidation of alcohols to aldehydes. *Catalysis Today*, 315, pp. 126–137.

Marie, J., Dikdim, D., Gong, Y., Bertrand, G., Marie, J., Zhao, X., Ma, N., Yang, M. and Bosco, J., 2019. Peroxymonosulfate improved photocatalytic degradation of atrazine by activated carbon/graphitic carbon nitride composite under visible light irradiation. *Chemosphere*, 217, pp. 833–842.

Mokhtar, N. M., Lau, W. J., Ismail, A. F. and Veerasamy, D., 2015. Membrane distillation technology for treatment of wastewater from rubber industry in Malaysia. *Procedia CIRP*, 26, pp. 792–796.

Niu, P., Qiao, M., Li, Y., Huang, L. and Zhai, T., 2018. Distinctive defects engineering in graphitic carbon nitride for greatly extended visible light photocatalytic hydrogen evolution. *Nano Energy*, 44, pp. 73–81.

Nuengmatcha, P., Chanthai, S., Mahachai, R. and Oh, W. C., 2016. Sonocatalytic performance of ZnO/graphene/TiO$_2$ nanocomposite for degradation of dye pollutants under ultrasonic irradiation. *Dyes and Pigments*, 134, pp. 487–497.

Oh, K. S., Leong, Y. C., Janet, Poh, P. E., Chong, M. N. and Lau, E. V., 2018. A review of greywater recycling related issues: Challenges and future prospects,in Malaysia. *Journal of Cleaner Production*, 171, pp. 17–29.

Olea-Mejia, O., Contreras-Bulnes, R., Zamudio-Ortega, C. M., Morales-Luckie, R. A. and López-Castañares, O. O. C. R., 2014. Scanning electron microscopy and energy dispersive spectroscopy microanalysis applied to human dental specimens under laser irradiation for caries prevention. *Microscopy: Advance in Scientific Research and Education*, pp. 70–77.

Ong, C. B., Ng, L. Y. and Mohammad, A. W., 2018. A review of ZnO nanoparticles as solar photocatalysts: Synthesis, mechanisms and applications. *Renewable and Sustainable Energy Reviews*, 81(8), pp. 536–551.

Pang, Y. L. and Abdullah, A. Z., 2012. Fe^{3+} doped TiO_2 nanotubes for combined adsorption – sonocatalytic degradation of real textile wastewater. *Applied Catalysis B: Environmental*, 129, pp. 473–481.

Pang, Y. L., Abdullah, A. Z. and Bhatia, S., 2010. Optimization of sonocatalytic degradation of Rhodamine B in aqueous solution in the presence of TiO_2 nanotubes using response surface methodology. *Chemical Engineering Journal*, 166, pp. 873–880.

Piarapakaran, S., 2018. Selangor in hot water over water crisis. *News Straights Times,* [online] 23 March. Available at: <https://www.nst.com.my/opinion/letters/2018/03/348275/selangor-hot-water-over-water-crisis> [Accessed 19 August 2018]

Pokhrel, N., Vabbina, P. K. and Pala, N., 2016. Sonochemistry: Science and engineering. *Ultrasonics Sonochemistry*, 29, pp. 104–128.

Purswani, J., Lopez-Lopez, C., Martin-Pascual, J., Martinez-Toledo, M. V., Munio, M. M. and Poyatos, J. M., 2014. Toxic effect of H_2O_2 in H_2O_2/UV , photo-Fenton and heterogeneous photocatalysis systems to treat textile wastewater. *Desalination and Water Treatment*, 56(11), pp. 3044-3053.

Qin, J. and Zeng, H., 2017. Photocatalysts fabricated by depositing plasmonic Ag nanoparticles on carbon quantum dots/graphitic carbon nitride for broad spectrum photocatalytic hydrogen generation. *Applied Catalysis B: Environmental*, 209, pp. 161–173.

Qiu, P., Park, B., Choi, J., Thokchom, B., Pandit, A. B. and Khim, J., 2018. A review on heterogeneous sonocatalyst for treatment of organic pollutants in aqueous phase based on catalytic mechanism. *Ultrasonics Sonochemistry*, 45, pp. 29–49.

Rout, T. K., and Singh, R. K., 2011. Pyrolysis of coconut shell.

Rout, T., Pradhan, D., Singh, R. K. and Kumari, N., 2016. Exhaustive study of products obtained from coconut shell pyrolysis. *Journal Of Environmental Chemical Engineering*, 4(3), pp. 3696-3705.

Saini, R. D., 2017. Textile organic dyes: Polluting effects and elimination methods from textile waste water. *International Journal of Chemical Engineering Research*, 9(1), pp. 975–6442.

Shimizu, N., Ogino, C., Mahmoud, F. D. and Murata, T., 2007. Sonocatalytic degradation of methylene blue with TiO_2 pellets in water. *Ultrasonics Sonochemistry*, 14, pp. 184–190.

Song, L., Zhang, S., Wu, X. and Wei, Q., 2012. A metal-free and graphitic carbon nitride sonocatalyst with high sonocatalytic activity for degradation methylene blue. *Chemical Engineering Journal,* 184, pp. 256–260.

Soni, A., Tiwari, A. and Bajpai, A. K., 2013. Removal of malachite green from aqueous solution using nano-iron oxide-loaded alginate microspheres: Batch and column studies. *Research On Chemical Intermediates*, 40(3), pp. 913–930.

Stat-Ease, 2018. *Fit Summary (RSM/MIX Model Selection).* [online] Available at: <https://www.statease.com/docs/v11/contents/analysis/fit-summary.html> [Accessed 22 March 2019].

Sun, Z., Wang, H., Wu, Z. and Wang, L., 2018. G-C_3N_4 based composite photocatalysts for photocatalytic CO_2 reduction. *Catalysis Today*, 300, pp. 160–172.

Suslick, K. S., 1986. Organometallic sonochemistry. *Advances in Organometallic Chemistry*, 25(C), pp. 73–119.

Suslick, K. S., 1990. Sonochemistry. *Science (New York)*, 247, pp. 1439–1445.

Taer, E., Taslim, R., Putri, A. W., Apriwandi, A. and Agustino, A., 2018. Activated carbon electrode made from coconut husk waste for supercapacitor application. *International Journal of Electrochemical Science*, 13, pp. 12072–12084.

Thue, P. S., Lima, E. C., Sieliechi, J. M., Saucier, C., Dias, S. L. P., Vaghetti, J. C. P., Rodembusch, F. S. and Pavan, F. A., 2017. Effects of first-row transition metals and impregnation ratios on the physicochemical properties of microwave-assisted activated carbons from wood biomass. *Journal Of Colloid And Interface Science*, 486, pp. 163–175.

Thurston, J. H., Hunter, N. M., Wayment, L. J. and Cornell, K. A., 2017. Urea-derived graphitic carbon nitride (u-g-$C_3N_{4)}$ films with highly enhanced antimicrobial and sporicidal activity. *Journal Of Colloid And Interface Science*, 505, pp. 910–918.

Toyoda, M., Tsumura, T., Tryba, B., Mozia, S. and Janus, M., 2016. Carbon materials in photocatalysis. *Chemistry And Physics Carbon*, 31, pp. 171–267.

Tripathi, A. and Narayanan, S., 2018. Impact of TiO_2 and TiO_2/g-C_3N_4 nanocomposite to treat industrial wastewater. *Environmental Nanotechnology, Monitoring & Management*, 10, pp. 280-291.

Tyborski, T., Merschjann, C., Orthmann, S. and Yang, F., 2013. Crystal structure of polymeric carbon nitride and the determination of its process-temperature-induced modifications. *Journal Of Physics: Condensed Matter*, 25(39), pp. 1-7.

Wang, A., Wang, C., Fu, L., Wong-Ng, W. and Lan, Y., 2017. Recent advances of graphitic carbon nitride-based structures and applications in catalyst, sensing, imaging, and LEDs. *Nano-Micro Letters*, 9(47).

Wang, F., Wang, Y., Feng, Y., Zeng, Y., Xie, Z. and Zhang, Q., 2018. Novel ternary photocatalyst of single atom-dispersed silver and carbon quantum dots co-loaded with ultrathin g-C_3N_4 for broad spectrum photocatalytic degradation of naproxen. *Applied Catalysis B : Environmental*, 221, pp. 510–520.

Wang, R., Lu, K.Q., Tang, Z.R. and Xu, Y.J., 2017. Recent progress in carbon quantum dots: synthesis, properties and applications in photocatalysis. *Journal of Materials Chemistry A*, 5(8), pp. 3717–3734.

Xu, H. Y., Wu, L. C., Zhao, H., Jin, L. G., and Qi, S. Y., 2015. Synergic effect between adsorption and photocatalysis of metal-free g-C_3N_4 derived from different precursors. *PLOS ONE*, 10(11), pp. 1–20.

Yu, Y., Zhu, Z., Fan, W., Liu, Z., Yao, X., Dong, H., Li, C. and Huo, P., 2018. Making of a metal-free graphitic carbon nitride composites based on biomass carbon for efficiency enhanced tetracycline degradation activity. *Journal of the Taiwan Institute of Chemical Engineers*, 89, pp. 151–161.

Yue, B., Li, Q., Iwai, H., Kako, T. and Ye, J., 2011. Hydrogen production using zinc-doped carbon nitride catalyst irradiated with visible light. *Science and Technology of Advanced Materials*, 12(3), pp. 1-7.

Yue, X., Yi, S., Wang, R., Zhang, Z. and Qiu, S., 2016. Cadmium sulfide and nickel synergetic co-catalysts supported on graphitic carbon nitride for visible-light-driven photocatalytic hydrogen evolution. *Scientific Reports*, 6, pp. 1–9.

Zaman, S., Zhang, K., Karim, A., Xin, J., Sun, T. and Gong, J. R., 2017. Sonocatalytic degradation of organic pollutant by SnO_2/MWCNT nanocomposite. *Diamond and Related Materials*, 76, pp. 177–183.

Zhang, K., Zhang, F. J., Chen, M. L. and Oh, W. C., 2011. Comparison of catalytic activities for photocatalytic and sonocatalytic degradation of methylene blue in present of anatase TiO_2-CNT catalysts. *Ultrasonics Sonochemistry*, 18(3), pp. 765–772.

Zhang, L., Jin, Z., Huang, S., Huang, X., Xu, B. and Hu, L., 2019. Bio-inspired carbon doped graphitic carbon nitride with booming photocatalytic hydrogen evolution. *Applied Catalysis B : Environmental*, 246, pp. 61–71.

Zhao, Z., Sun, Y. and Dong, F., 2014. Graphitic carbon nitride based nanocomposites: A review. *Nanoscale*, 1(1), pp. 2–4.

Zhou, C., Sun, X., Yan, J., Chen, B., Li, P., Wang, H., Liu, J., Dong, X. and Xi, F., 2017. Thermo-driven catalytic degradation of organic dyes by graphitic carbon nitride with hydrogen peroxide. *Powder Technology*, 308, pp. 114–122.

Zhu, B., Xia, P., Ho, W. and Yu, J., 2015. Isoelectric point and adsorption activity of porous g-C_3N_4. *Applied Surface Science*, 344, pp. 188–195.

Zhu, L., Meng, Z., Park, C. Y., Ghosh, T. and Oh, W. C., 2013. Characterization and relative sonocatalytic efficiencies of a new MWCNT and CdS modified TiO_2 catalysts and their application in the sonocatalytic degradation of rhodamine B. *Ultrasonic Sonochemistry*, 20(1), pp. 478-484.

APPENDICES

APPENDIX A: The Calibration Curve for Malachite Green

$y = 0.1548x - 0.0561$
$R^2 = 0.9985$
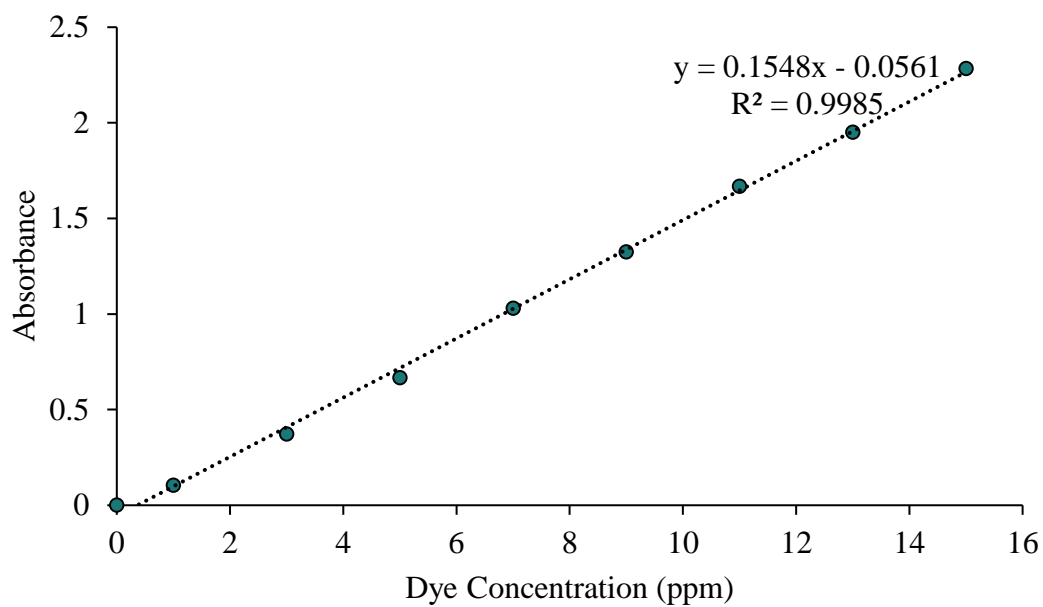
APPENDIX B: The Calibration Curve for Methyl Orange

$y = 0.0308x - 0.0163$
$R^2 = 0.996$
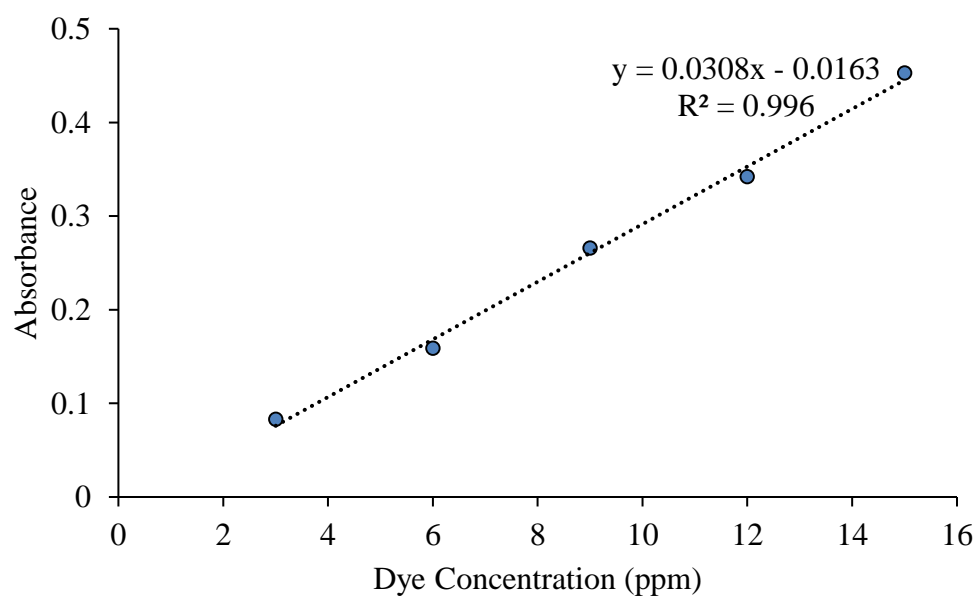
APPENDIX C: The Calibration Curve for Acid Orange G